1290

UNIVERSIDADE DE
COIMBRA

Tomás Dinis Ruaz Ferreira

Torque and Temperature Analysis in TAFSW of Low Carbon Steels

Dissertação no âmbito do Mestrado Integrado Engenharia Mecânica, na área de Produção e Projeto orientada pela Professora Doutora Dulce Maria Esteves Rodrigues e pelo Professor Doutor Carlos Miguel Almeida Leitão e apresentada ao Departamento de Engenharia Mecânica da Faculdade de Ciências e Tecnologia da Universidade de Coimbra

Outubro de 2020

1290
FACULDADE DE
CIÊNCIAS E TECNOLOGIA
UNIVERSIDADE Đ
COIMBRA

Torque and Temperature Analysis in TAFSW of Low Carbon Steels

Submitted in Partial Fulfilment of the Requirements for the Degree of Master in Mechanical Engineering in the specialty of Production and Project.

Análise do Binário e Temperatura em *TAFSW* de Aços de Baixo Teor em Carbono

Author
Tomás Dinis Ruaz Ferreira

Advisors
Professora Doutora Dulce Maria Esteves Rodrigues
Professor Doutor Carlos Miguel Almeida Leitão

Jury

President	**Professora Doutora Cristina Maria Gonçalves dos Santos** **Professora Auxiliar da Universidade de Coimbra**
Vowels	**Professor Doutor Ivan Rodolfo Pereira Garcia de Galvão** **Professor Adjunto do Instituto Superior de Engenharia de Lisboa**
Advisors	**Professor Doutor Carlos Miguel Almeida Leitão** **Investigador Doutorado da Universidade de Coimbra**

Coimbra, October, 2020

Blood, Sweat and Respect.

The first two you give, the last one you earn.

Dwayne « The Rock » Johnson

ACKNOWLEDGEMENTS

The current dissertation is the culmination of several years of academic career. However, the completion of this journey was only possible thanks to the collaboration and support of some people, to whom I cannot fail to give my recognition.

To professor Dulce Rodrigues and professor Carlos Leitão, advisors of the current dissertation, for all the guidance, knowledge, motivation, patience and good work environment provided during the development of this work without which it would be impossible to achieve this feat.

To my late father, Fernando, who I hope to be proud of its son achievement, and to my mother, Miquelina, for all the help, support and knowledge. I would like to extend my thanks also to my brothers, as well as to the remaining close relatives.

To all my long-time friends for the support, trust, respect, presence, friendship and funny moments during the past years.

To all the friends that my university path allowed me to meet. It has been quite a journey, and I'm grateful for their presence, support and amazing stories who changed to me to be what I am now.

To my incredible work college David and to the amazing Sree for all the patience, support, good work environment and funny moments which made the development of this dissertation even more special. I also would like to thank professor Ivan Galvão for its support.

A final thanks goes to FEDER funds for sponsoring the research where the subject of this dissertation is included, through Portugal 2020 (PT2020), by the Competitiveness and Internationalization Operational Program (COMPETE2020) and national funds through the Portuguese Foundation for Science and Technology, under the projects: UID/EMS/00285/2020, POCI-01-0145-FEDER-00763 and Friction 4.0 (POCI-01-0145-FEDER-032089).

Abstract

The prediction of the thermomechanical conditions developed in Tool Assisted Friction Spot Welding (TAFSW) is very important in order to produce strong and defect free welds. The objective of current dissertation is to contribute for the industrial implementation of this process, by analysing the torque and the temperature outputs, in order to assess the thermomechanical conditions developed during welding. With this objective, a series of welding tests were performed, using five different base materials, including two mild steels (DC01 and DC05), two high strength steels (HC420 and DP600) and a galvanized steel (DX200). The process parameters considered in the analysis were the tool diameter and the tool rotational speed. The temperature evolution during welding was acquired using a thermographic camera and the torque was obtained from the welding machine. Post processing of the torque and temperature raw data enabled to determine the maximum torque (M_{max}), the stabilized torque (M_{stb}) and the maximum temperature (T_{max}) corresponding to each welding test. The modelling of the torque and temperature data, with analytical models from the literature, was also conducted.

It was found that both the tool diameter and the tool rotational speed have a strong influence on the maximum and the stabilized torque values, as well as on the maximum temperature registered during welding. According to the present results, meanwhile the increase in the tool diameter results in a strong increase of the torque values, the increase in the rotational speed leads to a decrease in torque values. The increase in tool diameter, as well as the increase of the rotational speed, both promote an increase in the maximum temperatures reached during welding. Actually, for the maximum temperature, a threshold value of 1100 ºC was determined, irrespective to the base materials. The threshold temperature was mainly registered when welding with the larger tool diameter (16 mm) and/or the highest rotational speed (1500 rpm). The maximum temperature also showed to be less sensitive to the tool diameter when welding at the highest rotational speed. The fitting of the experimental results with analytical models, from the literature, showed high accuracy of the models in predicting all the process output values, especially for torque.

Keywords: Torque, Temperature, TAFSW, Modelling, Steel, Lap Joints.

Resumo

A previsão das condições termomecânicas desenvolvidas em *Tool Assisted Friction Spot Welding* (*TAFSW*) é muito importante para produzir soldaduras fortes e sem defeitos. O objetivo da presente dissertação é contribuir para a implantação industrial deste processo, por meio da análise dos valores de binário e da temperatura obtidos durante o mesmo, a fim de avaliar as condições termomecânicas desenvolvidas durante a soldadura. Com este objetivo, foram realizados uma série de ensaios de soldadura, utilizando cinco materiais de base diferentes, incluindo dois aços macios (DC01 e DC05), dois aços de alta resistência (HC420 e DP600) e um aço galvanizado (DX200). Os parâmetros de processo considerados na análise foram a velocidade de rotação e o diâmetro da ferramenta. A evolução da temperatura durante a soldadura foi medida com recurso a uma câmara termográfica, e o binário obtido na máquina de soldadura. O pós-processamento dos dados obtidos de binário e temperatura possibilitou determinar os valores de binário máximo (M_{max}), binário estabilizado (M_{stb}) e de temperatura máxima (T_{max}) correspondentes a cada ensaio de soldadura. A modelação dos dados de binário e temperatura, com modelos analíticos da literatura, também foi realizada.

Verificou-se que tanto o diâmetro da ferramenta como a velocidade de rotação têm forte influência nos valores de binário máximo e binário estabilizado, assim como nos valores de temperatura máxima registrada durante a soldadura. De acordo com os presentes resultados, enquanto que o aumento no diâmetro da ferramenta resulta num forte aumento dos valores de binário, o aumento da velocidade de rotação leva a uma diminuição dos mesmos. O aumento do diâmetro da ferramenta, assim como o aumento da velocidade de rotação, promovem um aumento nas temperaturas máximas atingidas durante a soldadura. Na verdade, para a temperatura máxima, foi determinado um valor limite de 1100 ºC, independente dos materiais de base. Esta temperatura limite foi registrada principalmente para soldaduras com o maior diâmetro da ferramenta (16 mm) e/ou para a maior velocidade de rotação (1500 rpm). A temperatura máxima também apresentou menor sensibilidade à variação do diâmetro da ferramenta ao soldar na maior velocidade de rotação. O ajuste dos resultados experimentais com modelos analíticos da literatura, demostrou elevada precisão dos modelos na predeterminação dos valores das variáveis obtidas no processo, principalmente para binário.

Palavras-chave: Binário, Temperatura, *TAFSW*, Modelação, Aço, Junta Sobreposta.

Contents

LIST OF FIGURES viii

LIST OF TABLES x

LIST OF SYMBOLS AND ACRONYMS / ABBREVIATIONS xii
  Symbols xii
  Acronyms/Abbreviations xii

1. INTRODUCTION 1

2. STATE OF THE ART 3
  2.1. The welding process 3
  2.2. Torque and temperature analysis 7

3. EXPERIMENTAL PROCEDURE 11
  3.1. Base materials 11
  3.2. Tools 12
  3.3. Process parameters 13
  3.4. Temperature acquisition 14
  3.5. Post-processing procedures 15
    3.5.1. Torque data 15
    3.5.2. Temperature data 16

4. ANALYSIS OF RESULTS 19
  4.1. Process output analysis 19
    4.1.1. Torque evolution with process parameters 19
    4.1.2. Temperature evolution with process parameters 21
    4.1.3. Torque and temperature correlation 23
  4.2. Modelling torque and temperature in TAFSW 26
    4.2.1. The analytical models 26
    4.2.2. Evolution of torque with Gω 27
    4.2.3. Modelling the torque 28
    4.2.4. Modelling the temperature 31
  4.3. Sensitivity analysis 34
    4.3.1. Torque versus process parameters 34
    4.3.2. Temperature versus process parameters 38

5. CONCLUSIONS 41
  5.1. Future works 42

BIBLIOGRAPHY 43

APPENDIX A 46

LIST OF FIGURES

Figure 2.1 – Axial and rotational movement of the welding tool a) Friction Stir Welding (FSW) b) Friction Stir Spot Welding (FSSW) c)... 4

Figure 2.2 - Examples of different types of pin tools a) pin-less tool b) 5

Figure 2.3 - Relationship between variables with physical effects overlapped (Colligan & Mishra, 2008)... 8

Figure 3.1 - True stress-strain curves of the base materials 12

Figure 3.2 - Pin-less tools used in the tests 12

Figure 3.3 - Thermographic Camera layout 14

Figure 3.4 – Torque curve example during TAFSW process 16

Figure 3.5 - Temperature curve example during TAFSW process 17

Figure 4.1 - Influence of process parameters on maximum torque.................................... 20

Figure 4.2 - Influence of process parameters on stabilized torque..................................... 21

Figure 4.3 - Influence of process parameters on temperature 22

Figure 4.4 - Temperature vs maximum torque for DC01 steel 23

Figure 4.5 - Temperature vs stabilized torque for DC01 steel 24

Figure 4.6 - Plots of temperature vs maximum torque (left)/stabilized torque (right) for the materials tested (DC05; DX200; HC420; DP600).. 25

Figure 4.7 - Gω analysis for maximum torque... 28

Figure 4.8 - Gω analysis for stabilized torque 28

Figure 4.9 - Fitting graphs for the maximum torque.. 29

Figure 4.10 - Fitting graphs for the stabilized torque... 30

Figure 4.11 - Km values for maximum and stabilized torque.. 31

Figure 4.12 - Fitting graphs for the temperature 33

Figure 4.13 - Individual influence of process parameters in maximum/stabilized torque .. 35

Figure 4.14 – Tri-dimensional graphs for maximum torque 36

Figure 4.15 – Tri-dimensional graphs for stabilized torque 37

Figure 4.16 – Tri-dimensional graphs for temperature 39

Figure 4.17 - Individual influence of process parameters in temperature 40

LIST OF TABLES

Table 3.1 - Chemical composition of the base materials [%] 11

Table 3.2 - Process parameters considered in the welding experiments 13

Table 4.1 - Process parameters for tri-dimensional graphs 34

Table A.1 - Maximum temperature, maximum torque and stabilized torque values obtained from experimental tests 46

LIST OF SYMBOLS AND ACRONYMS / ABBREVIATIONS

Symbols

$\mathbf{M}_{max}$ – Maximum Torque

$\mathbf{M}_{stb}$ – Stabilized Torque

$\mathbf{T}_{max}$ – Maximum Torque

Acronyms/Abbreviations

FSW – Friction Stir Welding

FSSW – Friction Stir Spot Welding

TAFSW – Tool Assisted Friction Spot Welding

FCTUC – Faculdade de Ciências e Tecnologia da Universidade de Coimbra

1. INTRODUCTION

In 1991, Wayne Thomas, at The Welding Institute (TWI), developed the Friction Stir Welding (FSW) technology. This solid-state joining technology came as an alternative to fusion welding processes, since it enables to avoid typical defects associated with most base materials melting. It has also lower operative costs due to a higher energy efficiency, the absence of consumables and shielding gases, as well as, the simplicity of the joint preparation. The FSW process is able to produce linear joints, in different configurations and for sheets with different thicknesses, by using a rotating tool, inserted in the abutting interface between the base materials to be joined. The non-consumable tool generates the heat required for softening the base materials and generates the weld by stirring the material around its axis. This process was initially applied in the joining of aluminium alloys, extending later to polymers and steels.

Friction Stir Spot Welding (FSSW) was later invented by Sakano et al., (2001). This process is able to produce spot welds in overlapped joints, is based on the same operative principles of the FSW technology, simply suppressing the linear motion of the tool. The Tool Assisted Friction Spot Welding (TAFSW) process is a variant of the FSSW technology in which the conventional tool, composed by a shoulder and a pin, is replaced by a plain pinless tool. This adaptation was firstly applied to the FSW technology, in order to enable the linear lap welding of steels with reduced tool wear, being posteriorly designated as Tool Assisted Friction Welding (TAFW). Later it was found that the pin removal had important benefits in spot welding by significantly reducing the upward material flow, which enables to avoid lap welding defects such as hooking.

In any solid state welding process, the prediction of the thermomechanical conditions developed during welding is very important in order to produce strong and defect free welds. However, in TAFSW, to achieve this objective, there is still an important lack of information on this subject. So, the objective of current dissertation is to contribute for the industrial implementation of the TAFSW process, by analysing the torque and the temperature process outputs, in order to assess the thermomechanical conditions developed during welding. To achieve this objective, a large number of welding tests were performed, using five different base materials and a diversified range of welding parameters. The five base materials were steels with varying mechanical properties, chemical composition and, in one case, surface finishing. Namely, two mild steels (DC01 and DC05), two high strength steels (HC420 and DP600) and a galvanized steel (DX200) were used in the investigation. The process parameters considered in the analysis were the tool diameter and the tool rotational speed. The temperature evolution during welding was acquired using a thermographic camera and the torque was obtained from the welding machine. In the dissertation are described all the procedures developed for the post-processing of the raw torque and temperature data, are displayed and analysed the experimental results, and finally, the modelling of the torque and temperature data, with analytical models from the literature, is performed. With these procedures, the influence of the process parameters on the thermomechanical conditions developed during welding was assessed.

Based on the above description, the dissertation was divided in 5 chapters. After the brief introduction in current chapter, Chapter 2 provides a state of the art related to the FSW and TAFSW processes, focusing on spot welding and torque/temperature studies. On chapter 3 is described the experimental procedure, as well as the post processing of the raw data obtained from the welding tests. In Chapter 4 are presented and discussed the experimental results. Finally, in Chapter 5 are presented the main conclusions from current work and are made propositions for future works.

2. STATE OF THE ART

This section is dedicated to resume the current state of the art associated with the theme developed during this dissertation. It is divided in two sections. The first one is focused on introducing the welding process, with especial attention on the TAFSW variant. The second section provides an overview of the literature on torque and temperature, evaluating each of the process outputs individually and also the interconnection between both.

2.1. The welding process

In both Friction Stir Welding (FSW) and Friction Stir Spot Welding (FSSW), regardless of the type of tool used, the welding principles are the same. As shown in Figure 2.1, a rotating tool is plunged into the base materials (Figure 2.1 a)) and the heat generated by friction and plastic deformation softens the material around the tool, facilitating the material flow. The tool rotational movement promotes the mixing (Stir) of the base materials and, consequently, the bonding of the plates. In FSW (Figure 2.1 b)), alongside the rotation, the tool also has a traverse movement, producing linear welds. This process is considered to be more energy efficient than its alternative welding processes, providing good weld proprieties by enabling to avoid many of the defects associated with the fusion welding processes, at lower operative costs (Shen et al., 2019).

In FSW, process parameters such as the plunging speed, the tool rotational speed, the tool traverse speed, the dwell time and the tool geometry, have important influence on the final weld proprieties. In conventional FSW, it is used a cylindrical tool, composed by a shoulder and a pin, to promote the stirring of the base materials. Some examples of pin configurations are presented in Figure 2.2 a). Recently, a FSW related technique was proposed, in which the pin is suppressed from the tool leaving a plain shoulder tool, also known as pinless tool (Figure 2.2 b)). This FSW related process, which was labelled Tool Assisted Friction Welding (TAFW) by Mira-Aguiar et al., (2016), was primarily developed to enable the welding of high strength materials, such as steels, by minimizing tool wear. Soon the TAFW process proved to have many other advantages, over conventional FSW, since it enables to supress the keyhole left by the pin at the end of the welds. Mira-Aguiar et al., (2016) also concluded that the TAFW technique enables to obtain very good quality linear welds, at very high welding speeds and low tool wear.

Spot welding is an old technique considered to be a faster, more economical and practical way of joining overlapped sheets than linear welding. The most common method to produce spot welds consists in applying local pressure and heat, using copper electrodes that transmit electrical current through the overlapped sheets, generating heat by Joule effect. The material melts and then solidifies, while under the pressure exerted by the electrodes, creating a weld. This process is called Resistance Spot Welding (RSW) (Shen et al., 2019).

The Friction Stir Spot Welding (FSSW) technology is a variation of the FSW process, firstly implemented by Mazda Motor Corporation in 1993, in which the traverse movement of the tool is suppressed, enabling only the plunging and retraction of the tool into the two lap plates, in order to produce "spot" welds (Figure 2.1 c)). FSSW is a relatively recent method that starts to be considered as a good alternative to RSW by offering many advantages, not only from the environmental and economic points of view, due to the reduced energy consumption, but also from a practical perspective, since it enables to produce comparable or superior weld strength with better consistency than RSW (Shen et al., 2019) for a variety of metals and non-metals, non-weldable by RSW, already being used in the automobile, shipbuilding and aerospace industries. The development of advanced tool materials has made possible to apply the FSSW technology to the spot joining of thin steel sheets as well (Rai et al., 2011). For these reasons, FSSW is gaining considerable interest for replacing conventional spot-welding methods.

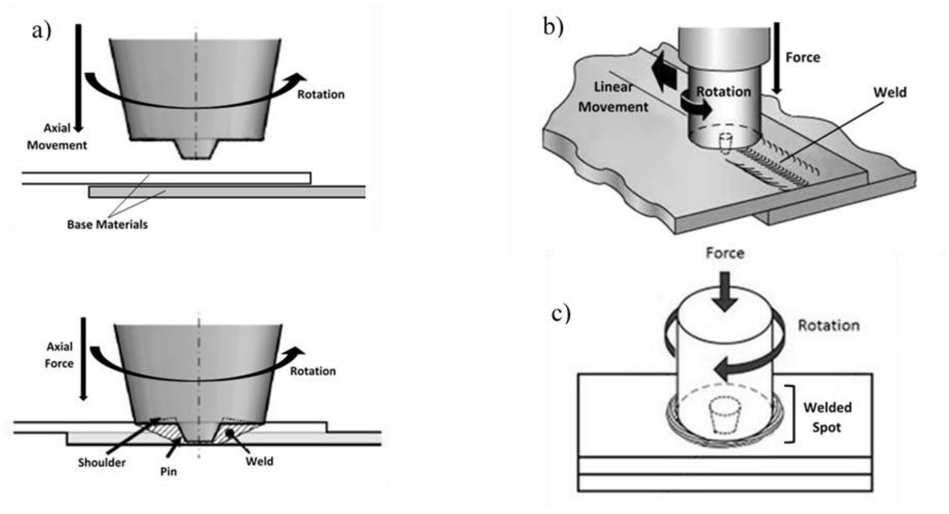

Figure 2.1 – Axial and rotational movement of the welding tool a) Friction Stir Welding (FSW) b) Friction Stir Spot Welding (FSSW) c)

Despite the many advantages of this spot welding technology, FSSW still has some drawbacks to be solved, such as avoiding the hooking defect formation and the keyhole left by tool pin (similarly to FSW) (Yazdi et al., 2019). These defects may lead to reduced joint strength (Cox et al., 2012; Mousavizade & Pouranvari, 2019) by creating stress concentration zones and making it difficult for corrosion control, potentially leading to failure. The application of pinless tools was also included in spot welding in 2009 (Shen et al., 2019) and has received increasing attention in the most recent years, being later designated as Tool Assisted Friction Spot Welding (TAFSW). It was found that the TAFSW alternative could mitigate the problems associated with conventional FSSW. TAFSW has an ability to weld very thin material sheets (1 mm thick) in short weld cycle times, which can improve the joining quality, reducing the formation of cracking. The main difference between the FSSW and TAFSW processes is the suppression of base materials stirring, across the interface to be bonded, due to the absence of the pin from the tool. Excessive stirring can lead to considerable material upward flow, at the base materials interface, which is set to be the main cause for the formation of the hook defect. Suppressing the stirring effect can improve the joint strength (De Leon & Shin, 2016).

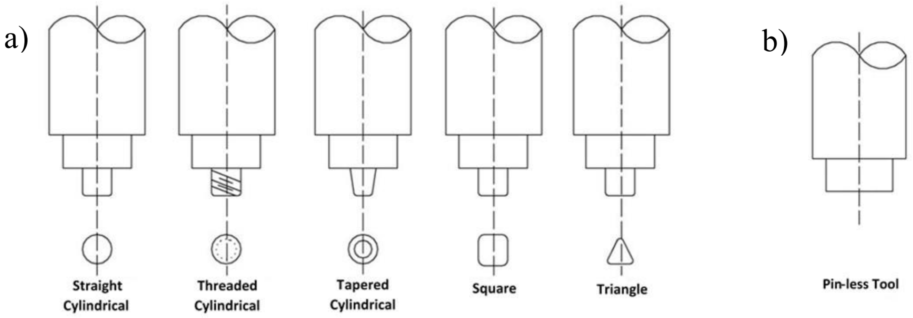

Figure 2.2 - Examples of different types of pin tools a) pin-less tool b)

As explained before, in opposition to FSSW, the TAFSW technique uses tools composed only by a shoulder, without a pin. The shoulder however can have surface features, instead of a flat area, which will promote a beneficial increase of the material flow and friction, leading to higher temperatures, as claimed by Tozaki et al., (2010) and Bakavos et al., (2011). In TAFSW, however, due to the suppression of material stir (Andrade et al., 2018), the bonding is provided by atomic diffusion mechanism associated with high pressures (Mira-Aguiar et al., 2016). Similarly to FSSW, the weld proprieties in TAFSW are determined by the tool geometry (diameter and surface features), as well as by process parameters such as the plunging time and depth, the welding time (dwell time) and the base material proprieties (Andrade et al., 2019). As in FSSW, the TAFSW operation can also be executed in position or force control. In the first case, a plunging depth is set and maintained during the dwelling period. In the second case, a force is set for the dwelling period.

Many researchers have studied the effect of the tool geometry and of the process parameters on the mechanical properties of the friction stir spot welds. Shen et al. (2019) postulated that increasing the tool rotational speed and the dwell time would increase the tensile/shear strength of the spot welds. They also concluded that there is a direct correlation between the effective weld width and the weld strength. This assumption was confirmed by Yazdi et al. (2019). Lakshminarayanan et al. (2015) concluded that, in FSSW, the dwell time is the main parameter in determining the joints properties, followed by the rotational speed and by the plunge depth.

Cox et al. (2014) studied the welding of aluminium alloys with pinless tools and concluded that the tool rotation speed and the dwell time were the dominating factors determining the joints strength. They also concluded that the higher the rotational speed and/or the longer the dwell time, the more severe the hooking defect.

A series of studies were also developed on the welding of steels with galvanized coatings. Baek et al., (2010) analysed welds produced by Friction Stir Spot Welding (FSSW) and concluded that the galvanized layer is expelled from the centre region of the joint. Mira-Aguiar et al., (2016) concluded that the zinc has an important influence on the contact conditions at the tool-workpiece material interface, in TAFW, affecting the thermo-mechanical conditions developed during welding.

2.2. **Torque and temperature analysis**

Torque and temperature are intrinsically connected. However, not only the torque and temperature evolutions during welding are not well known, but also the relationship between these two process outputs continues to be a topic of research, due to the lack of systematized information on this subject.

When the rotating tool makes contact with the base material, during the plunging phase, it generates a mechanical response in the form of torque. Simultaneously, there is an increase in temperature, due not only to the friction between the tool and the base material, but also to the plastic deformation promoted by the tool. According to Awang & Mucino, (2010), in FSSW, the friction work at the interface of the tool and the workpiece generates the most energy, which is about 96.84%, while the plastic deformation corresponds to 3.14%. The torque values oscillate during the welding process in order to guarantee the rotational speed set to the tool, as well as the axial force (in force control) or the plunge depth (in position control). In either FSSW or TAFSW, during the plunging stage, the torque increases, alongside with the temperature, until reaching a peak value. When approaching the end of the plunging stage, the material softening, associated with the temperature increase, allows the torque to decrease, reaching a constant value which is kept during the dwell period. At this point, the temperature also stabilizes in a maximum value.

There is an important concept that relates torque and temperature, and lies on the relative velocity between the tool and the material which is then associated with the friction and plastic work (Schmidt et al., 2004). This physical concept is known as slipping/sticking contact conditions. Throughout the welding process, while the tool is in contact with the workpiece, the interaction between the first and the former results in either a relative movement between both, designated as slipping, or a solidary movement of the tool with the adjacent soften base material, designated as sticking. Deductively, the slipping condition leads to friction, and the sticking condition leads to material flow. Considering a fixed workpiece, if the contact condition between the rotating tool and the base material is predominantly sticking, this will promote plastic work on the contact interface. During the welding process, the predominance of each contact condition varies and it is frequently unclear in FSSW/TAFSW (and FSW) if a sticking or slipping condition occurs at the tool interface (Bakavos et al., 2011).

Colligan & Mishra (2008) developed a conceptual model that described the relation between process parameters/variables and heat generation related process outputs in FSW. In Figure 2.3 is represented the scheme, elaborated by the authors, for representing the relationship between each of the process variables and the process outputs, represented in boxes with solid borders. The physical effects associated with each process variable are represented in boxes with dashed borders. The direct and inverse relationships are signalled by plus (+) and minus (-), respectively.

From the scheme, it is possible to conclude that the torque increases for larger tool diameters and also for larger pin lengths, in the case of FSSW process. The rotational and linear speed of the tool also promote variations on the torque values in a way that the increase in rotational speed and/or a decrease in transverse speed will decrease the torque. However, the linear translation of the tool has little influence on the torque behaviour as concluded by Leitão et al. (2012) and also concluded by Arora et al. (2009).

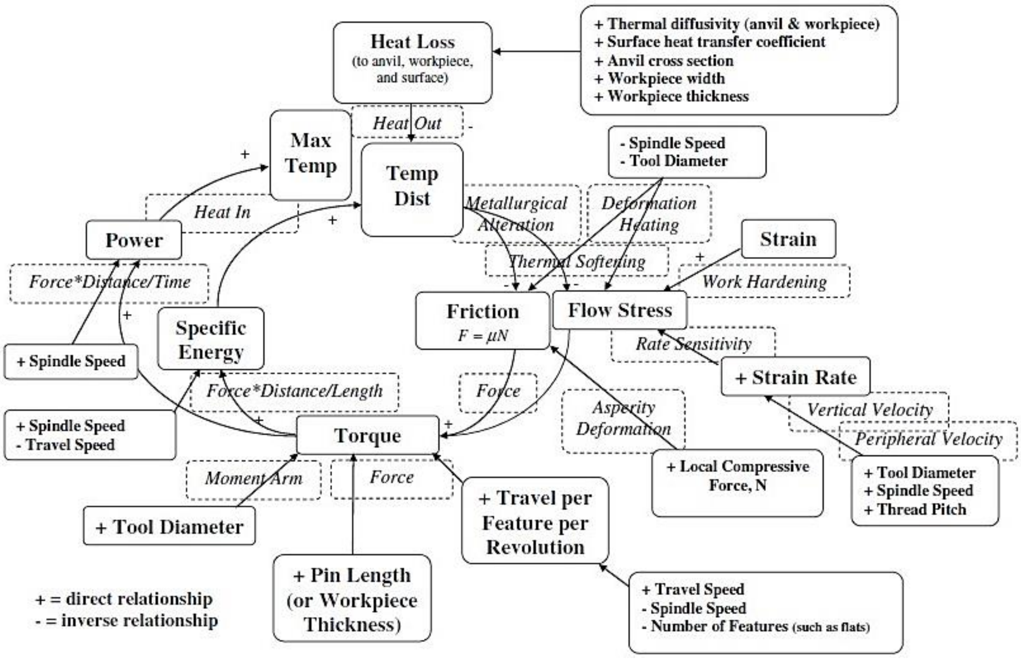
Heat Loss (to anvil, workpiece, and surface)
+ Thermal diffusivity (anvil & workpiece)
+ Surface heat transfer coefficient
+ Anvil cross section
+ Workpiece width
+ Workpiece thickness
Heat Out
Max Temp
Temp Dist
- Spindle Speed
- Tool Diameter
Heat In
Power
Metallurgical Alteration
Deformation Heating
Strain
Thermal Softening
Work Hardening
Force*Distance/Time
Friction F = μN
Flow Stress
+ Spindle Speed
Specific Energy
Rate Sensitivity
+ Strain Rate
+ Spindle Speed
- Travel Speed
Force*Distance/Length
Force
Asperity Deformation
Vertical Velocity
Peripheral Velocity
Torque
Moment Arm
Force
+ Local Compressive Force, N
+ Tool Diameter
+ Spindle Speed
+ Thread Pitch
+ Travel per Feature per Revolution
+ Tool Diameter
+ Pin Length (or Workpiece Thickness)
+ = direct relationship
- = inverse relationship
+ Travel Speed
- Spindle Speed
- Number of Features (such as flats)

Figure 2.3 - Relationship between variables with physical effects overlapped (Colligan & Mishra, 2008)

In the current dissertation, our focus lies on the torque and temperature and the relationship between both. In general, an inverse relation is usually established between these output process parameters, i.e. when the maximum temperature values increase, the torque values decrease.

The correlation between torque and temperature is provided by the heat generation associated with friction and plastic work, as mentioned before. As the temperature increases, the material begins to soften, facilitating the material flow, causing a decrease in torque values. This state occurs for elevated temperatures, below the melting point of the material. The tool geometry and rotational speed have both a high influence in the relation between torque and temperature, changing the way that heat is generated and also by modifying the material flow behaviour. As explained by Freeney et al. (2006), lower tool rotational speed means that less heat is generated by friction, decreasing material softening and consequently increasing the flow stress between tool and base material, which will increase the torque values (Andrade et al., 2020b; Arora et al., 2009; Leitão et al., 2012a). The base material also has a strong influence on the process output values. According to Leitão et al. (2012), which performed studies on FSW, there is strong influence of the base materials plastic proprieties on the torque. Andrade et al., (2020a) concluded that material flow during welding is determined by the base material plastic properties, in first, and by the contact conditions at the tool/workpiece interface, in second. However, an increase in torque values with the increase of tool diameter can occur when welding for the same rotational speed. Andrade et al., (2020b) concluded that the increase of the torque with the tool dimensions has to be related to the increase of the amount of material stirred by the tool.

The torque output passively responds to the set inputs such as rotational speed and tool diameter, and the temperature evolution. Torque is also considered the most accurate way to determine the energy spend on the welding process (Longhurst et al., 2010). Several works analysed the viability of using the tool torque as a process response to the thermomechanical conditions (Andrade et al., 2020b; Cox et al., 2014).

The temperature as an important role in material proprieties. The monitoring of the temperature achieved during the welding could be decisive to accomplish good weld proprieties, by reducing defects and increasing joint strength. According to Jedrasiak & Shercliff, (2019) and Khosa et al., (2010), friction welding contact conditions are self-stabilizing, i.e. as temperature rises, the flow stress falls and the heat generation reduces, so conditions converge on a state of thermal balance between material softening and heat generation. Andrade et al., (2019), found that the main factors influencing the frictional heat generation in TAFSW are, by order of importance, the tool diameter, the tool rotation speed and the presence of low melting point coatings. Santella et al., (2012), who performed FSW of galvanised steels, observed that the presence of a galvanised coating in steel sheets reduced the welding temperatures, up to 110 °C, when compared to uncoated welds produced under the same welding conditions. Mazzaferro et al., (2015) and Mira-Aguiar et al., (2016), who also analysed galvanised steel welds, concluded that the galvanised coating melted during the welding process, working as a lubricant at the tool-plates interface, which prevented base material stirring and lowered the welding temperatures. Zuzarte et al., (2018) also concluded that presence of galvanized coatings on the surface of the sheets influence the generation of heat.

Andrade et al., (2019), who analysed the influence of the process parameters and of the base material properties in the thermomechanical conditions developed during TAFSW of steels, concluded that for each tool diameter, there is a threshold in the maximum temperature that can be reached during welding, which increases with the tool diameter. When welding with the larger tool diameter (16 mm), no important differences in maximum temperature were registered, independently of the base material and tool rotation speed, indicating that a threshold in heat generation was attained for a value of 1100 ºC. The authors also concluded that for small tool diameters, the maximum welding temperature varies according to the base material and tool rotation.

Rodrigues et al., (2017), who analysed the process parameters and base materials influence in the heat generation conditions in TAFW of steels, concluded that the maximum temperatures were higher for the higher rotational speeds and tool diameters. A great influence of the base material characteristics was also observed by the authors, who concluded that the highest maximum temperatures were obtained for the steel with the highest mechanical strength. The authors also concluded that for coated steels, there was a decrease in maximum temperature values with the increase of the coat thickness.

3. EXPERIMENTAL PROCEDURE

Tool Assisted Friction Spot Welding (TAFSW) was performed, following standard procedures, in order to evaluate the torque and the temperature cycles associated with it, as well as the correlation between both. In the next, the base materials and the TAFSW process parameters used in the investigation are described. The procedures for process output analysis and temperature assessment are also explained.

3.1. Base materials

Being the world's most important engineering and construction material, steels are used in innumerous applications with the possibility of being recycled without loss of proprieties. In this work, five steels were used as base materials, including two mild steels, designated as DC01 and DC05, two high strength steels, designated as HC420 and DP600, and one galvanized steel, designated as DX200. The composition of each base material is presented in Table 3.1.

Table 3.1 - Chemical composition of the base materials [%]

Material	C	Mn	P	S	Si	Cr
DC01	0,050	0,210	0,016	0,008	0,010	0,030
DC05	0,003	0,140	0,007	0,002	0,010	0,010
DX200	0,019	0,210	0,014	0,004	0,008	0,000
HC420	0,095	1,440	0,013	0,013	0,410	0,000
DP600	0,145	1,650	0,040	0,008	0,900	0,500

To better illustrate the mechanical properties of the base materials, in Figure 3.1, are represented the true stress-strain curves for the five steels. From the figure, it is possible to conclude that the DC01 and DC05 steels, with 159 and 140 MPa yield strength (YS), respectively, and with 397 and 389 MPa ultimate tensile strength (UTS), respectively, were the lower strength steels, displaying very similar mechanical behaviour. On the other hand, the HC420 and the DP600 steels, with 400 MPa and 349 MPa yield strength, respectively, and 670 MPa and 800 MPa ultimate tensile strength, respectively, were the highest strength base materials, but displaying significantly different tensile behaviour. Finally, the DX200 steel, was the one with intermediate strength, displaying a yield strength of 277 MPa and an ultimate tensile strength of 435 MPa, close to that of the DC01 and DC05 steels.

The spot welds were produced using two overlapped squared sheets from each of these base materials, having 80 mm width and 1 mm thickness.

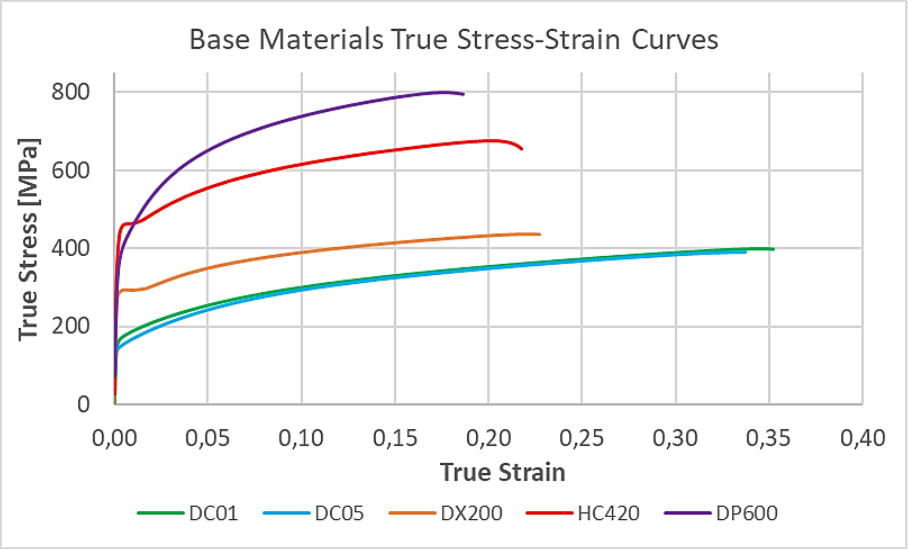

Figure 3.1 - True stress-strain curves of the base materials

3.2. **Tools**

Three plain pinless tools, with 10, 12 and 16 mm diameters, as schematized in Figure 3.2, were tested. In the next, the tools will be labelled, according to its diameter, as PL10, PL12 and PL16, respectively. The tools were made of Tungsten Carbide, in order to ensure high wear resistance, which is especially important when joining steels by TAFSW.

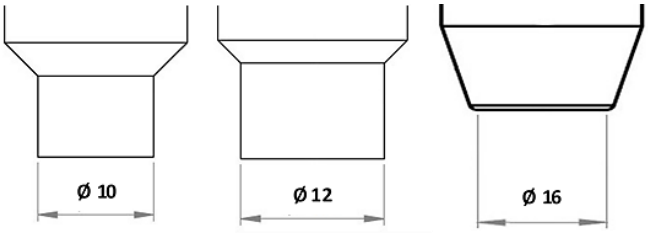

Figure 3.2 - Pin-less tools used in the tests

3.3. Process parameters

In order to have a large comprehensiveness on the torque and temperature evolution with welding conditions, several process parameters combinations were tested, as shown in Table 3.2. According to the table, spot welds were produced, for each steel, by using the three different tools and two different rotational speeds (870 and 1500 rpm). Welding was performed in position control, with a plunge depth of 0,5 mm (half the thickness of the upper sheet) and a plunging time (Pt) of approximately 4 seconds. To guarantee that stabilized heat generation was achieved in the welding process, the dwell period (Dt) was set to 60 seconds, making a total welding time of 64 seconds. The welding procedures were established following Andrade et al., (2019) recommendations.

Table 3.2 - Process parameters considered in the welding experiments

Materials	Rotational Speed [rpm]	Diameter [mm]	Dt [s]	Pt [s]
DC01	870	10	60	4
		12		
		16		
	1500	10		
		12		
		16		
DC05	870	10		
		12		
		16		
	1500	10		
		12		
		16		
DX200	870	10		
		12		
		16		
	1500	10		

		12		
		16		
HC420	870	10		
		12		
		16		
	1500	10		
		12		
		16		
DP600	870	10		
		12		
		16		
	1500	10		
		12		
		16		

3.4. Temperature acquisition

The temperature evolution during each welding test was recorded with a thermographic camera, model *FLIR A655sc*, positioned in direct line of sight from the welding apparatus, as represented in Figure 3.3. The camera was distanced 0,5 m from the contact point between the tool and the base material sheets, which was the selected region for temperature acquisition. The procedures for temperature acquisition were adopted from Andrade et al., (2019), who established a value of 0.95 for the emissivity of the five steels.

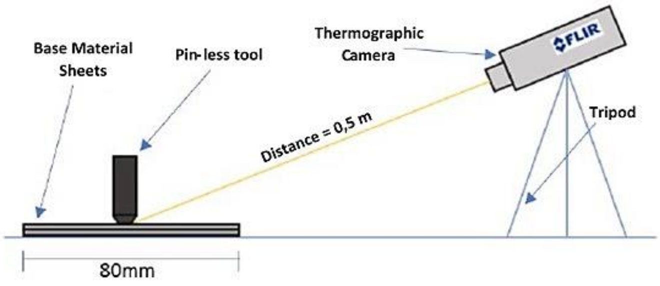
Base Material
Sheets
Pin-less tool
Thermographic
Camera
FLIR
Distance = 0,5 m
Tripod
80mm

Figure 3.3 - Thermographic Camera layout

3.5. Post-processing procedures

The welding machine, as well as the thermographic camera, registered large amount of raw data from which the information relevant for the investigation needed to be extracted. With this objective, the raw data was organized in MS Excel worksheets, which were programmed for the post-processing of the temperature and torque data, in order to determine the maximum torque and temperature values, as well as the stabilized torque.

3.5.1. Torque data

The torque evolution with time, registered by the welding machine, globally followed the same trend of the curve exemplified in Figure 3.4, obtained in the TAFSW of the DX200 steel, with the PL10 tool at 870 rpm. The time scale in the graphic gathers the plunging period, which was set to 4 seconds, and the welding time, which comprised the period between the end of the plunging and the beginning of the tool retraction, which was set to 60 seconds. As exemplified in the figure, all the torque versus time curves displayed important fluctuations, resulting from the high frequency of acquisition. This noise was suppressed from the curves using the “Smooth” function from Excel library. The curve resulting from this operation is also included in the graph.

In the torque versus time graphic, are identified the two main stages of the spot welding operation. The plunging phase, during which the torque rises due to the tool plunging into the cold base material, and the dwell phase. During the dwell phase, the torque starts decreasing, due to the softening of the base material under the heating promoted by the tool (stabilization period) reaching an almost constant value (stable period), until the end of the welding. The duration of the stabilization and stable periods was determined by calculating the instantaneous derivative of the torque (dM/dt), as plotted in the graph. In current work, it was assumed that the stabilization period ends when $-0,2 \leq dM/dt \leq 0.2$ Nm/s. After establishing the stabilization period, a stabilized torque value (M_{stb}) was determined, for each set of the welding conditions, by calculating an average of the torque values registered within this time interval. In the same way, the maximum torque (M_{max}) value, obtained from the Smooth curve, was also registered.

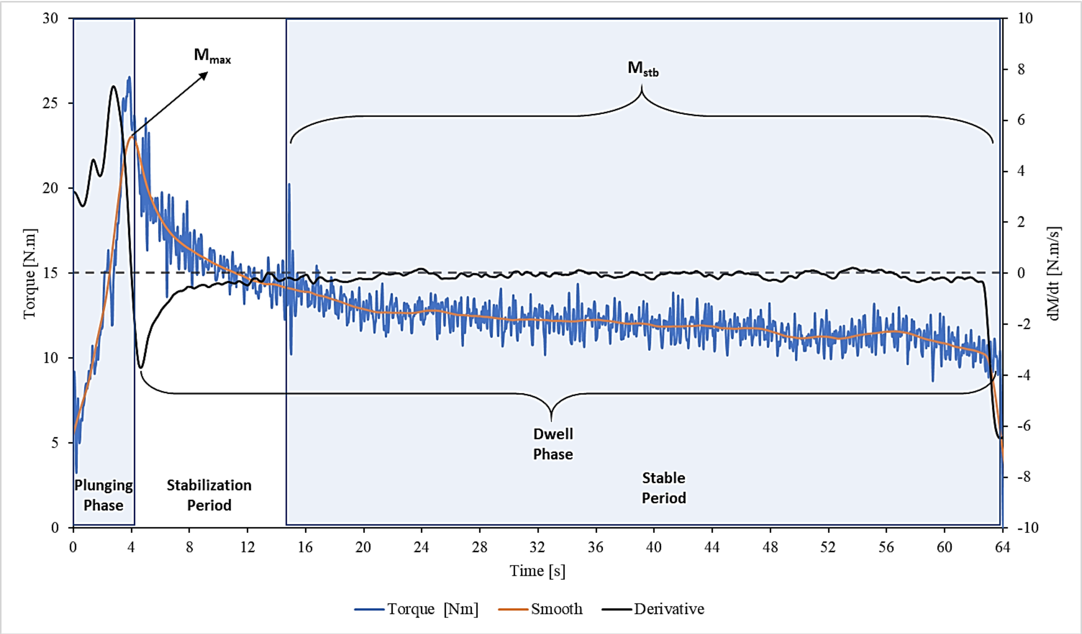

Figure 3.4 – Torque curve example during TAFSW process

3.5.2. Temperature data

Similarly to the torque, the temperature is also a very important process variable that needs to be monitored and studied. The temperature evolution with time (Thermal Cycle) determines the final microstructure and the mechanical strength of the welds. An example of a typical TAFSW thermal cycle is represented in Figure 3.5. Again, in this graph, the experimental curve, obtained from the thermographic camera, as well as and the calculated instantaneous derivative of the temperature (dT/dt) were plotted. Analysing the thermal cycle it is possible to identify three stages: (1) a heating period, during which the temperature rises, (2) a steady state period, during which the temperature remains almost constant, and (3) a cooling period, after the welding is finished, during which the temperature decreases. The instantaneous derivative of the temperature, serves the same purpose as the instantaneous derivative of the torque, i.e., it allows to identify the heating and steady state periods in the thermal cycle. In the temperature analysis, it was considered that a stabilized heat generation was achieved when $-4 \leq dT/dt \leq 4$ °C/s. A stabilized temperature value was then determined, for each set of welding conditions, by calculating the average of the temperature values registered within this time interval. In the thermal cycles, the stabilized temperature value coincides with the maximum temperature (T_{max}).

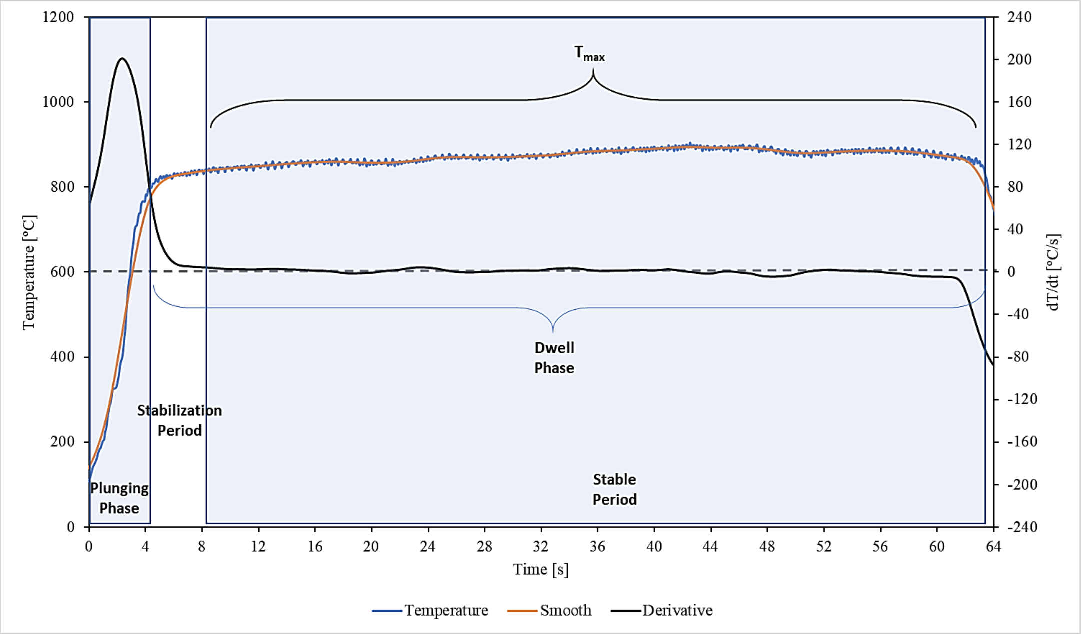

Figure 3.5 - Temperature curve example during TAFSW process

4. ANALYSIS OF RESULTS

In this chapter are displayed and analysed the torque and temperature results registered in the welding tests. The experimental data were then fitted with empirical models, from Andrade et al., (2020), in order to assess its suitability for the modelling of the process output data in the TAFSW of steels. In order to promote an intuitive understanding of the results, the chapter was divided in three sub-sections. In the first sub-section, it is analysed the evolution of the torque and temperature results with the process parameters (tool diameter and tool rotational speed) and base materials properties. In the second sub-section are shown the modelling results. Finally, in the last sub-section, tri-dimensional representations, comparing the obtained model surfaces with the experimental results are displayed and discussed.

4.1. Process output analysis

As mentioned in the experimental procedure section, the parameters of tool diameter and rotational speed were varied in the TAFSW of five different steels. In the next, the results of those tests are organized, not only with the objective of highlighting the influence of the process parameters on the torque and temperatures registered during welding, but also with the objective of establishing a comprehensive correlation between the two mentioned process output variables.

4.1.1. Torque evolution with process parameters

The analysis of the evolution of the torque values, with the process parameters, was performed by organizing the results in two graphs relative to the maximum (M_{max}) and stabilized (M_{stb}) torque values, respectively. In each graph, the variable under analysis is plotted as a function of the tool diameter used for performing the tests (10, 12 and 16 mm). The results corresponding to the tests performed with both rotational speeds had been included in each graph. Dashed and continuous intercept lines are used to group the 870 and 1500 rpm results, respectively.

Analysing Figure 4.1, relative to the evolution of M_{max} with the process parameters, it is possible to conclude that an increase in the maximum torque occurs when the tool diameter is increased, irrespective of the tool rotational speed and base material properties. However, the figure also shows that, for both rotational speeds, the increase in maximum torque with the tool diameter displays a non-linear behaviour, being sharper for high than for low tool diameters. This non-linear trend is independent of the base materials tested.

Comparing now the evolution of M_{max} with the rotational speeds, it is possible to conclude that, independently of the base material, higher maximum torque values were registered when welding with the lower rotational speed of 870 rpm. The figure also shows that, meanwhile for a given tool diameter, the maximum torque values relative to the welding at 1500 rpm are very similar, the same is not true for the results relative to the welding at 870 rpm. For this rotational speed, when welding with the larger tool diameter (16 mm), large differences in maximum torque values were registered when changing the base material. However, since the variation in maximum torque does not obey to any precise relation with base material properties (Figure 3.1), it can be considered that those differences may be related with errors in maximum torque acquisition.

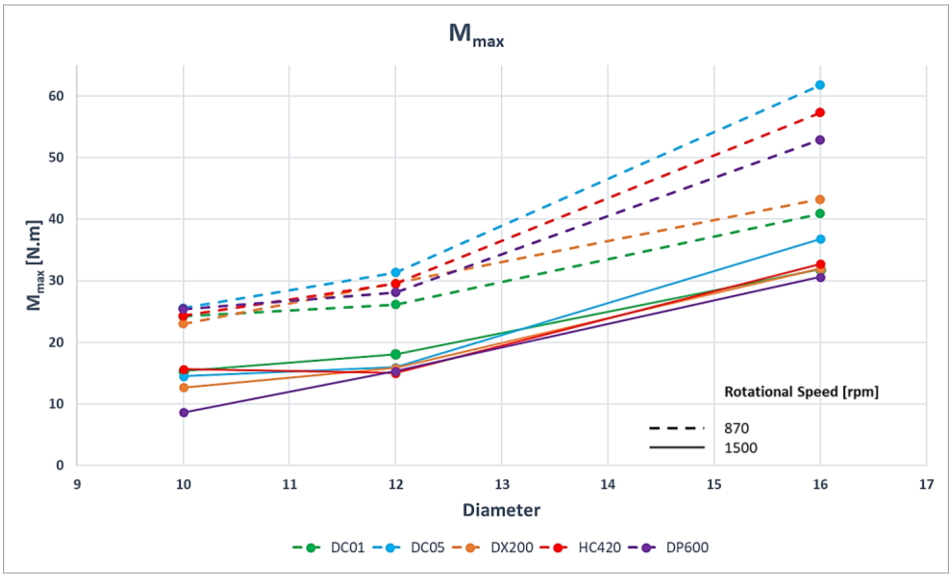

Figure 4.1 - Influence of process parameters on maximum torque

In Figure 4.2 is now represented the stabilized torque evolution with process parameters. Analysing the figure it is possible to conclude that, similarly to what was reported for the maximum torque, the stabilized torque values also increase with the increase in tool diameter and decrease with the increase in rotational speed. However, in opposition with that observed for the maximum torque evolution, there is a dissimilar trend in the stabilized torque evolution with the tool diameter, for the two rotational speeds. Meanwhile for 1500 rpm, a non-linear torque evolution with the tool diameter may be noticed, for 870 rpm, an almost linear evolution of the stabilized torque with the tool diameter can be observed. It is also important to enhance that, contrary to that reported when analysing the maximum torque evolution, no important differences in torque evolution/values may be reported when comparing the results relative to the different base materials. This observation supports the previous assumption that the differences in M_{max} may result from errors in torque acquisition.

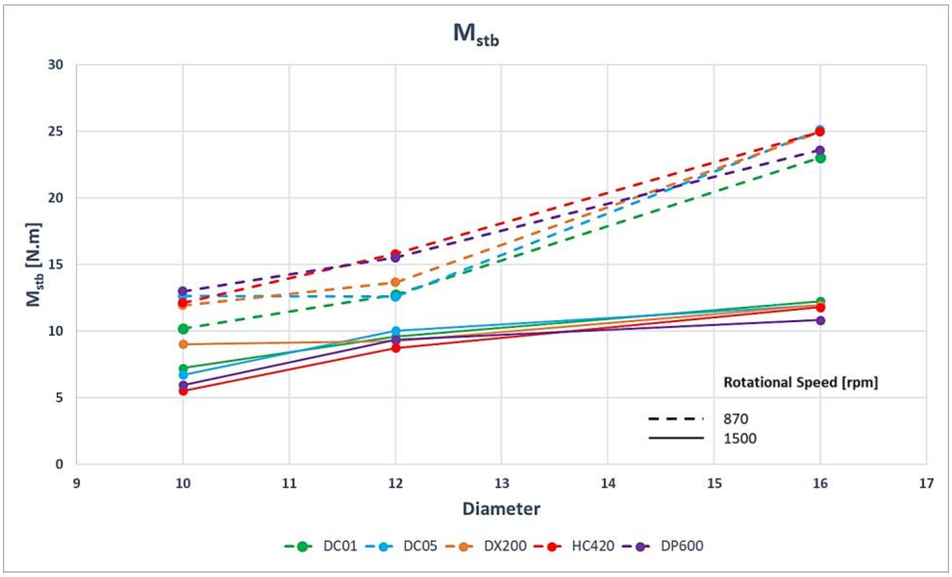

Figure 4.2 - Influence of process parameters on stabilized torque

4.1.2. Temperature evolution with process parameters

The evolution of the temperature values, with the process parameters, was plotted as a function of the tool diameter used for performing the tests (10, 12 and 16 mm), following the same roles used to organize the torque. The results corresponding to the tests performed with both rotational speeds had been included. Dashed and continuous intercept lines are used to group the 870 and 1500 rpm results, respectively.

In Figure 4.3 are represented the maximum temperature values. Analysing the figure it is possible to conclude that the trends in temperature evolution, with process parameters and base materials, are not similar to that reported for the torque evolution. For example, in the graph, for the low rotational speed of 870 rpm, it is noticeable a clear increase of the temperature with the tool diameter, for most of base materials, except the DX200 steel, for which lower temperatures were registered when welding with the PL16 tool. This general behaviour was expected since an increase in diameter will correspond to an increase in tool contact area, which will favour the heat input by friction and plastic deformation. For the lower rotational speed, strong differences in the maximum temperature values were registered between the base materials, contrary to that reported for the torque.

Comparing now the temperature results for the two rotational speeds, it is possible to conclude that, for most of the base materials, except the DP600 steel, the lower values of temperature correspond to the lower rotational speed, which, as shown before, also correspond to the higher torque values. For the DP600 steel, the maximum temperatures are very similar, irrespective of the rotational speed. The graphic also enables to observe that, irrespective of the process parameters and base materials properties, there is a threshold in heat generation, at 1100ºC.

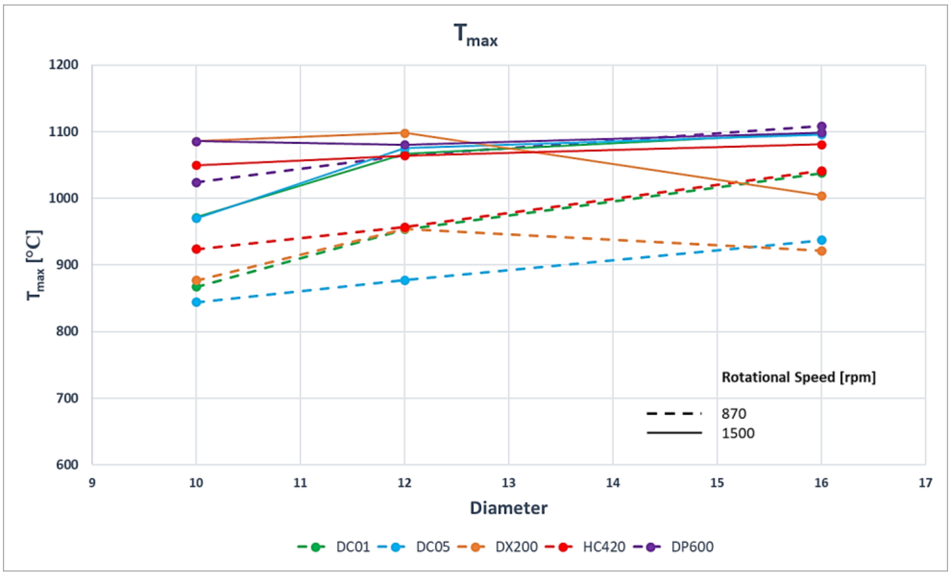

Figure 4.3 - Influence of process parameters on temperature

In Table A.1, from Appendix section, are listed all the maximum temperature, maximum torque and stabilized torque values achieved during the welding experiments.

4.1.3. Torque and temperature correlation

In order to analyse the torque evolution with the temperature, a series of graphs have been plotted, correlating the maximum and stabilized torque to the temperature, for the different base materials. In each graph are plotted all testing results related to the base material, organized as a function of the tool diameter (different symbols) and tool rotational speed (different colours). To enable a better understanding of the analysis, linear trend lines were included in each graph for each rotational speed.

In Figure 4.4 is represented the temperature correlation with the maximum torque for the DC01 steel. Analysing the results, it is possible to conclude that, meanwhile the increase in the rotational speed conducts to an increase in the temperature and to a decrease of the torque, the increase of the tool diameter, also promotes an increase in temperature, but this increase in temperature does not conduct to a decrease in the torque. According to Andrade et al., (2020a), this opposite trends in temperature to torque evolution with process parameters may be explained based on the concurrent influence of the temperature, and of the volume of material being stirred by the tool, on the torque. The same trends observed for the temperature vs. maximum torque evolution may be apperceived when analysing Figure 4.5, where is now represented the temperature vs stabilized torque correlation, for the DC01 steel. The main differences between Figure 4.4 and Figure 4.5 are related to the slope of the trend lines plotted in the graphs.

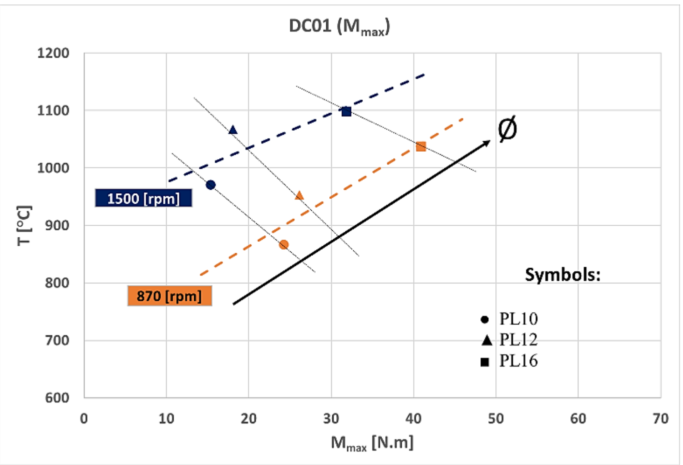

Figure 4.4 - Temperature vs maximum torque for DC01 steel

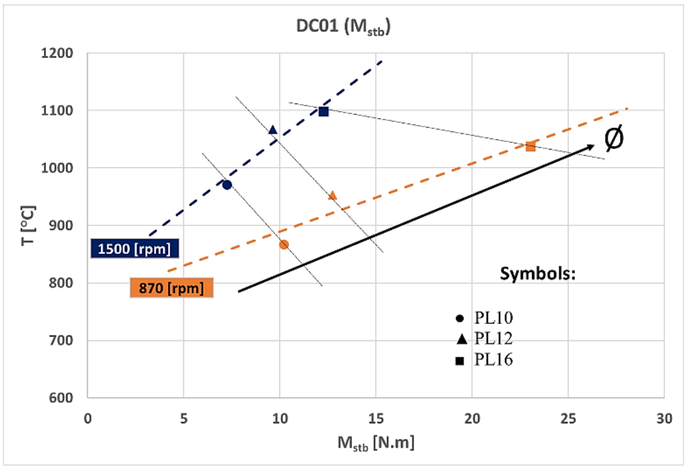

Figure 4.5 - Temperature vs stabilized torque for DC01 steel

The temperature vs maximum/stabilized torque graphs plotted for the remaining base materials are shown in Figure 4.6. Analysing the figure it is possible to conclude that the same general conclusions drawn for the DC01 steel, concerning the temperature vs torque evolution, are valid for the remaining base materials, except the coated steel (DX200). However, the figure also shows that, meanwhile the maximum and stabilized torques evolution with the temperature for the DC05 steel (Figures Figure 4.6 a) and b)) is very similar to that registered for the DC01 steel (Figures Figure 4.4 and Figure 4.5), for the HC420 and DP600 steels, this is not true. Actually, for the higher strength steels, the evolution of the maximum and stabilized torques with the temperature displays the same trend, i.e., the slope of the trend lines is the similar in the T vs M_{max} and T vs M_{stb} graphs. The figure also highlights that the differences in maximum temperature, when increasing the rotational speed, are much lower for the high strength steels than for the mild steels, again showing a threshold temperature at 1100 ºC.

Finally, analysing in Figure 4.6 c) and d) the results relative to the DX200 steel, it is possible to conclude that, for this base material, unlike that registered for the other steels, no important increase in temperature was registered when increasing the tool diameter. Actually, for the higher tool rotational speed (1500 rpm), the maximum temperature even decreased for the higher tool diameter. For this base material, both the maximum and the stabilized torque values evolved in a narrower range than for the other steels.

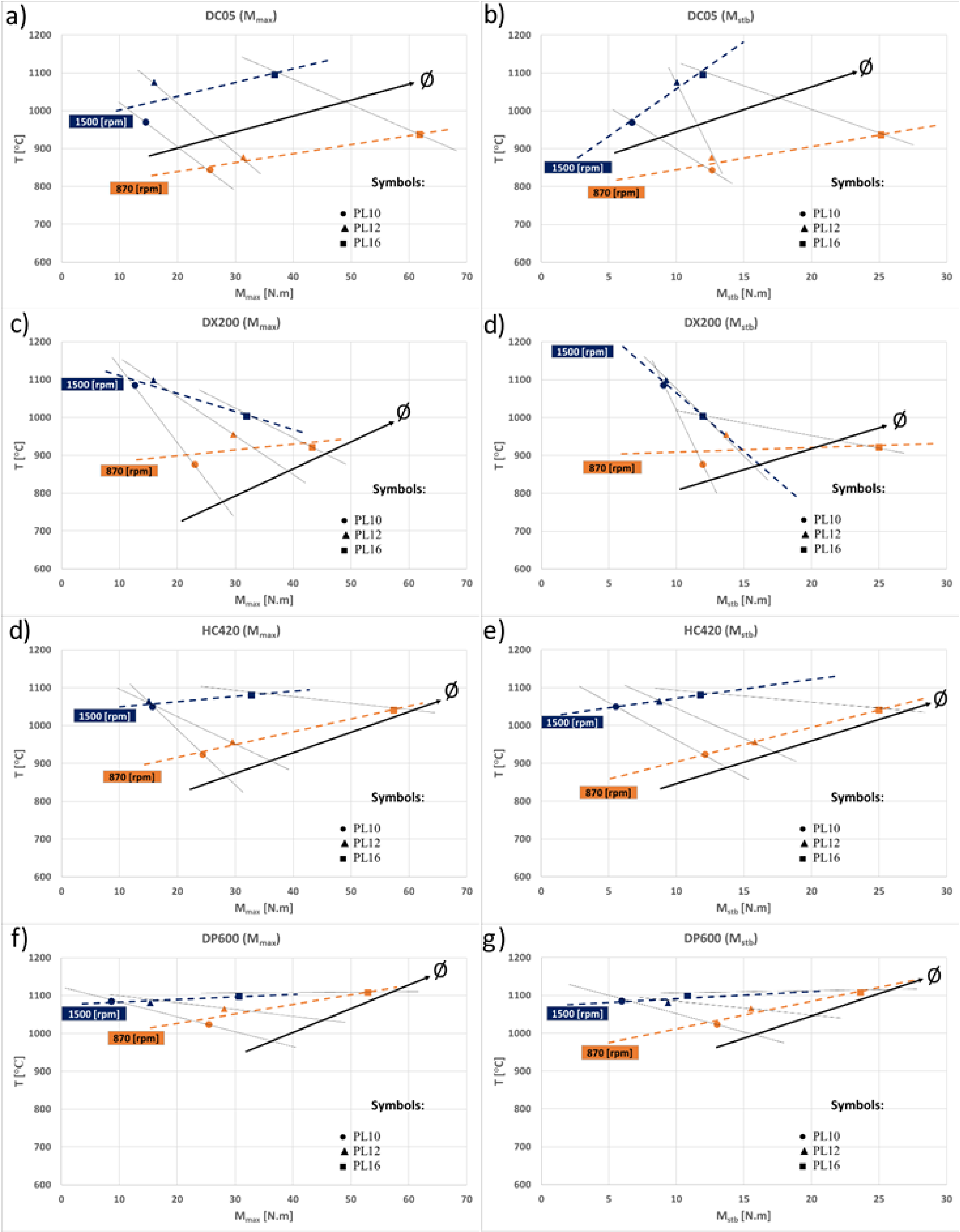

Figure 4.6 - Plots of temperature vs maximum torque (left)/stabilized torque (right) for the materials tested (DC05; DX200; HC420; DP600)

4.2. **Modelling torque and temperature in TAFSW**

In order to control and industrialize the technological processes, they must be well defined and predictable. In the case of the Tool Assisted Friction Spot Welding (TAFSW) technology, as well as in the FSW and other related processes, this means understanding and modelling the relation between process parameters and machine outputs, in order to control the heat generation and the material flow. Empirical models can be helpful in forecasting the evolution of the process outputs with the process parameters. This section is dedicated to test the feasibility of using the empirical models developed by Andrade et al., (2020b), in previewing the torque and temperature evolution, with process parameters, in TAFSW of steels. This analysis is of special relevance since the empirical models to be tested were developed based on data relative to the FSW of aluminium alloys.

4.2.1. The analytical models

The models developed by Andrade et al., (2020b) aim to predict the torque and temperature evolution with FSW process parameters (rotational speed, tool dimensions and transverse speed) and base material parameters (plates thickness). In the model, the tool dimensions are taken into account by using the geometry parameter (G), given by the equation

$$G = \frac{\pi}{4} {D_P}^2 + \pi D_P p_l + \frac{\pi}{4}(D_S - D_P)^2, \tag{4.1}$$

where p_l represents the pin length and D_S and D_P represent the tool shoulder and pin diameter, respectively. Since in TAFSW, pinless tools are used, the pin related factors of the equation are suppressed and the geometry parameter is simplified to

$$G = \frac{\pi}{4} {D_S}^2. \tag{4.2}$$

Andrade et al., (2020b) also proposed two coefficients for quantifying the torque and temperature evolution during welding. The torque (C_M) and temperature (C_T) coefficients are given by

$$C_M = \frac{G}{\omega} \sqrt[4]{vt}, \tag{4.3}$$

and,

$$C_T = \frac{G\omega}{\sqrt{vt}}. \tag{4.4}$$

In the previous equations, ω is the rotational speed, v is the traverse speed and t represents the thickness of the plates. Having in mind the very specific TAFSW characteristics, the traverse speed was withdrawn from both equations.

4.2.2. Evolution of torque with Gω

Andrade et al. (2020) concluded that the torque is greatly influenced by the tool dimensions and by the rotational speed. Based on this, the authors compared the evolution of torque with the product between the geometry parameter and the rotational speed (Gω). From this analysis, the authors proposed the C_M and C_T coefficients for modelling the torque and the temperature in FSW of aluminium alloys, respectively. The same type of analysis was performed in this work, for the maximum torque evolution in TAFSW of steels.

In Figure 4.7 is represented the maximum torque versus Gω for all the base materials tested in current work. Adopting the same procedure described in Andrade et al. 2020, the results were grouped as a function of the G parameter, which, in this work, is proportional to the three different tool diameters (10, 12 and 16 mm). The torque results associated with each G parameter group, which are distinguished in the graph by using different colours, were fitted using power functions. Once again it is noticeable the decrease of torque values with the increase in rotational speed, while an increase in G values promotes higher torques. Also, it is possible to observe that a great dispersion in maximum torque values was registered for tools corresponding to a G parameter of 200 mm^2, which leads to a Pearson correlation coefficient of 0,764. This dispersion was verified before, in Figure 4.1, especially for the PL16 tool at 870 rpm.

In Figure 4.8 is now represented a similar analysis, but this time for the stabilized torque. The fitting achieved, with R^2 values starting at 0,81, is better than that obtained for the maximum torque, which was expected due to the proximity of the experimental values obtained between the materials, as previewed in Figure 4.2. In the figure, it is also possible to observe the decrease of the torque, with the rotational speed, and the increase of the torque, with the geometry parameter, similarly to that reported for the maximum torque.

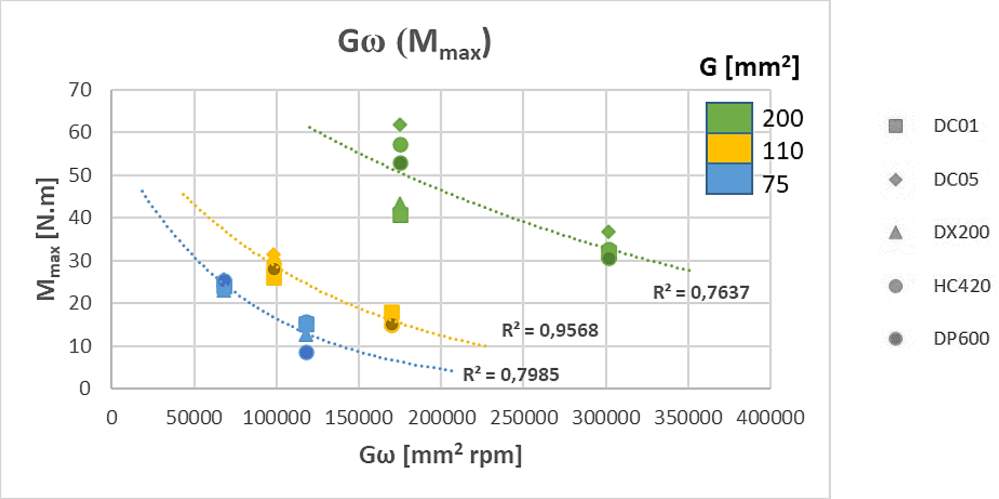

Figure 4.7 - Gω analysis for maximum torque

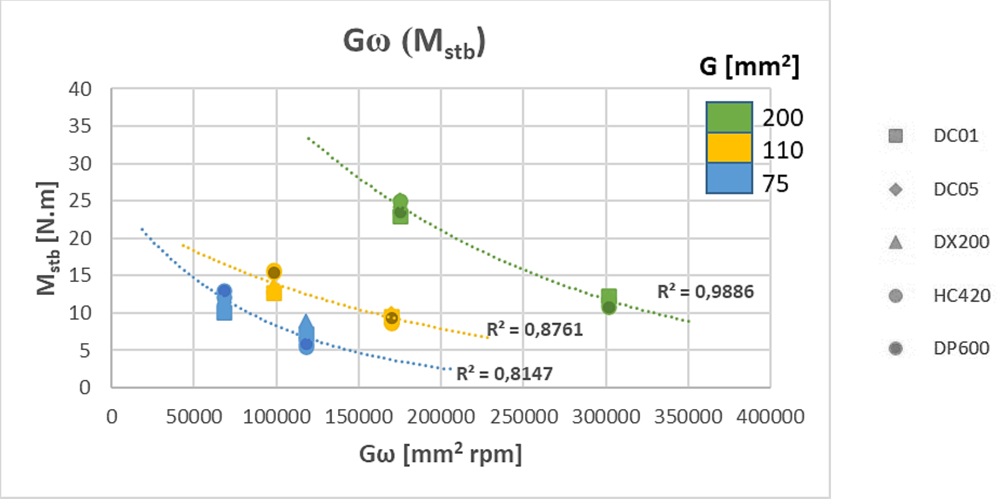

Figure 4.8 - Gω analysis for stabilized torque

4.2.3. Modelling the torque

In order to assess the suitability of the model for fitting the experimental results of torque, a series of graphs were plotted, for each of the base materials tested, in which the experimental results of maximum and stabilized torque were plotted against the CM coefficient. The data plotted was then fitted by linear regression, in order to determine the coefficient K_M of the empirical equation

$$M = K_M C_M \tag{4.5}$$

that relates the torque with the process parameters. In each graph, together with the fitting of equation (4.5), it is also plotted the Pearson correlation coefficient (R^2) value, which was used for assessing the accuracy of the fitting.

In Figure 4.9 are represented the fitting graphs obtained for the maximum torque. Analysing the figure, it is possible to conclude that a very good correlation between the experimental and analytical results ($R^2 > 0{,}97$) was obtained using the C_M coefficient proposed by Andrade et al., (2020b). The K_M values obtained, for the different steels, range between 172 and 221.

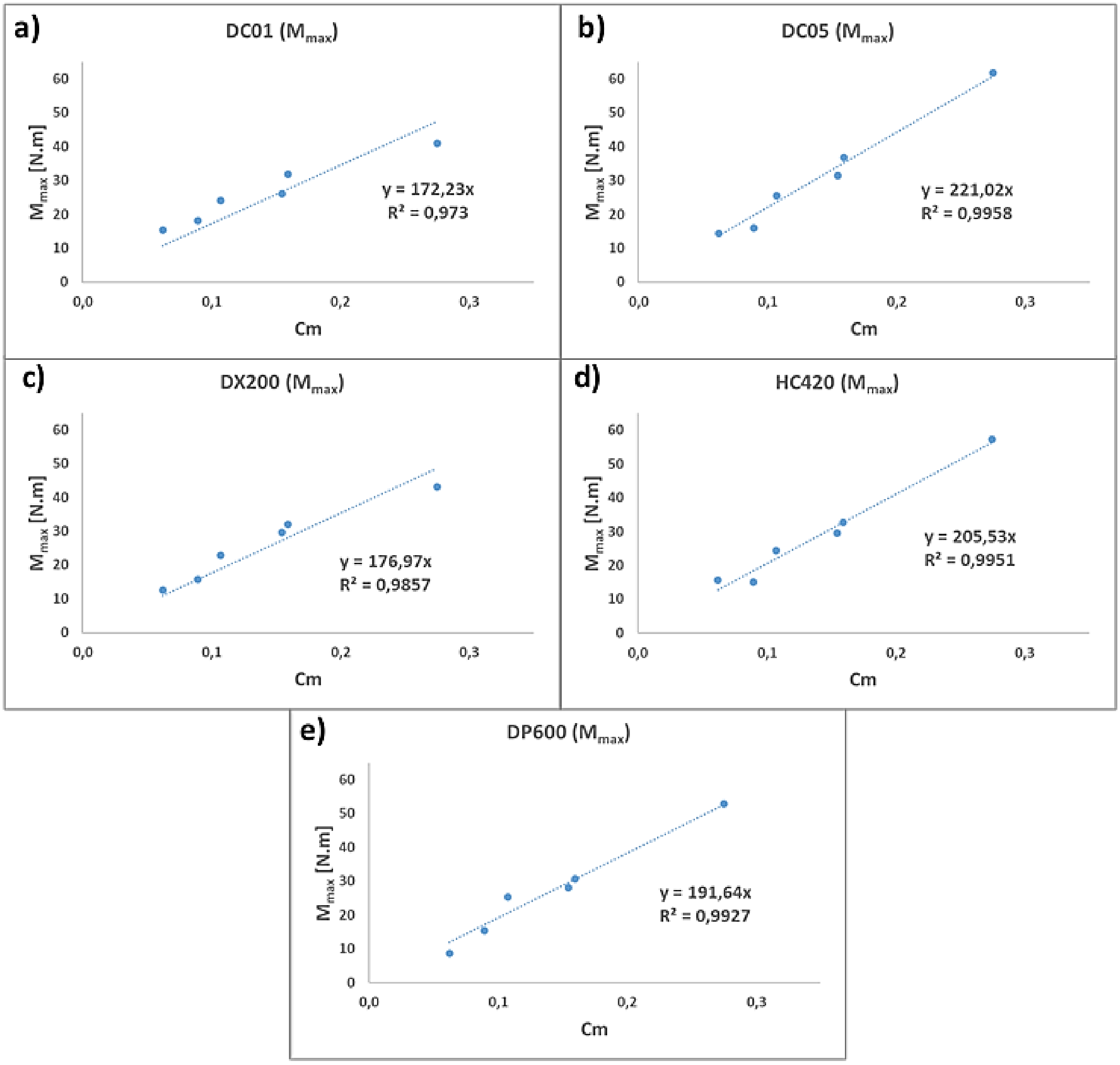

Figure 4.9 - Fitting graphs for the maximum torque

In Figure 4.10 are now correlated the experimental and analytical results obtained for the stabilized torque. Similarly to the maximum torque, a very good agreement between the experimental and analytical values was obtained ($R^2 > 0{,}97$). The K_M coefficient values determined for the stabilized torque range between 85 and 92.

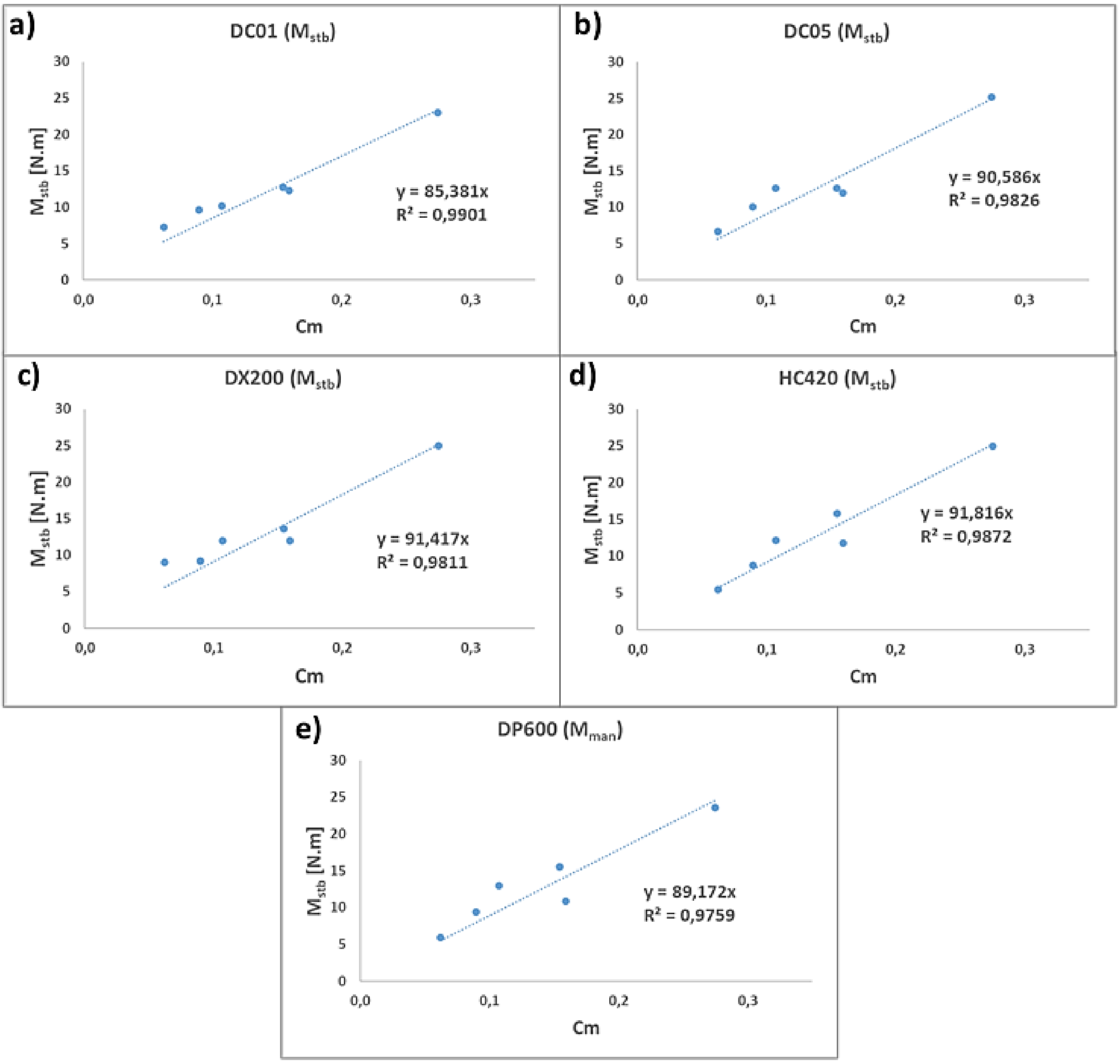

Figure 4.10 - Fitting graphs for the stabilized torque

In Figure 4.11 are compared the K_M values determined from the fitting of the maximum and stabilized torque values. A line representing the average of the K_M coefficients is also plotted in each graph. The figure shows that the K_M values for maximum torque have a great disparity, which will translate into a noticeable difference in the maximum torque evolutions for the materials, as shown in Figure 4.14. Some errors related to the maximum torque acquisition may also be influencing the K_M values, as mentioned above. However, for stabilized torque, the K_M values show a minor variation, which correlates to a very similar evolution throughout the different base materials, as verified in Figure 4.15

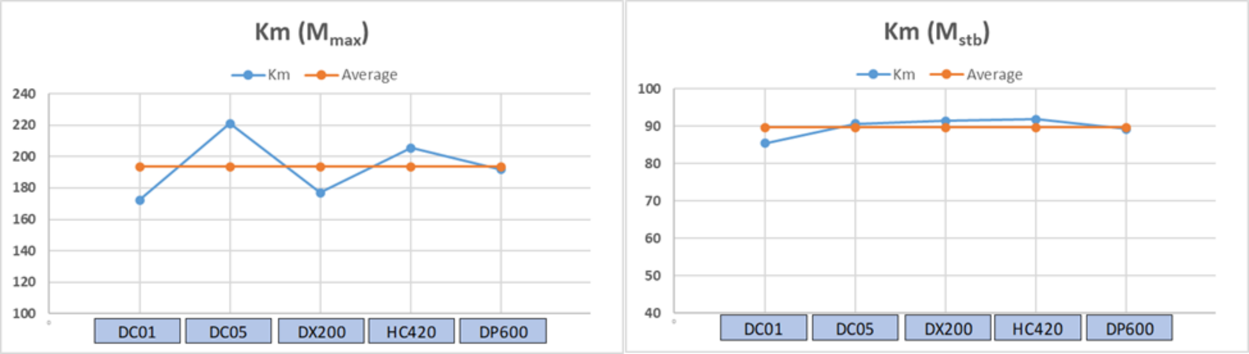

Figure 4.11 - Km values for maximum and stabilized torque

4.2.4. Modelling the temperature

As it was done when modelling the torque, the suitability of the temperature model for fitting the experimental results was assessed by plotting a graph, for each of the base materials tested, in which the experimental results of temperature were represented against the C_T coefficient. The data plotted was then fitted in order to determine the coefficients K_T and φ of the power equation

$$T = K_T {C_T}^{\varphi} \tag{4.6}$$

that relates the temperature with the process parameters. In each graph, together with the fitting of equation (4.6), it is also plotted the Pearson correlation coefficient value, which was used for assessing the accuracy of the fitting.

Taking into consideration the temperature results obtained (Figure 4.3) and also the results achieved by Andrade et al., (2019), it is possible to conclude that, for certain set of process parameters, the temperature reaches a threshold value of 1100 ºC. Andrade et al., (2020b) also considered the existence of a threshold temperature in aluminium, of 590 ºC, for C_T > 20000. A similar approach was adopted in this work, by considering

$$\begin{cases} T = K_T {C_T}^{\varphi} \ for\ C_T < 120000 \\ T = 1100\ ℃\ for\ C_T > 120000 \end{cases} \tag{4.7}$$

where for C_T values under 120000, the fitting equation is applied, while for C_T values above 120000 a threshold temperature of 1100 ºC is assumed. The C_T value of 120000 was obtained by visual analysis of the fitting graphs for the temperature (Figure 4.12).

In Figure 4.12 are compared the experimental and analytical results obtained for the temperature. A horizontal line is included in each graph, indicating the threshold temperature of 1100 ºC. The two conditions from (4.7) are represented in different colours. Analysing the figure, it is possible to conclude that the correlation between the experimental and analytical results is not as good as that obtained for the torque. In spite a satisfactory fitting was obtained for the DC01 and DC05 results (R^2 = 0,989 and 0,932, respectively), for the HC420 and DP600 results, the Pearson correlation coefficient ranged between 0,756 to 0,853. The DX200 registered a fitting value 0,864. However, it is important to remember that the temperature evolution with process parameters, registered for the DX200 steel (Figure 4.3), was different from that registered for the other steels.

In the figure it is also noticeable, for most materials, that the threshold condition is achieved for C_T values above 120000, as mentioned. However, some errors during temperature acquisition, may be influencing its correct measurement. An example of this can be seen for the DC05 steel, where the temperature measured for a C_T value of 123690 (threshold condition) was lower than the expected value of 1100 ºC, around 937 ºC. It is also important to remember that the boundary value defined for C_T of 120000 was set based on a visual analysis of experimental results, with all the inherent imprecision associated with it. Verifying the K_T values from the equations, it is concluded that the values achieved differ for each steel, contrary to the conclusion in Andrade et al., (2020b) for the aluminium alloys.

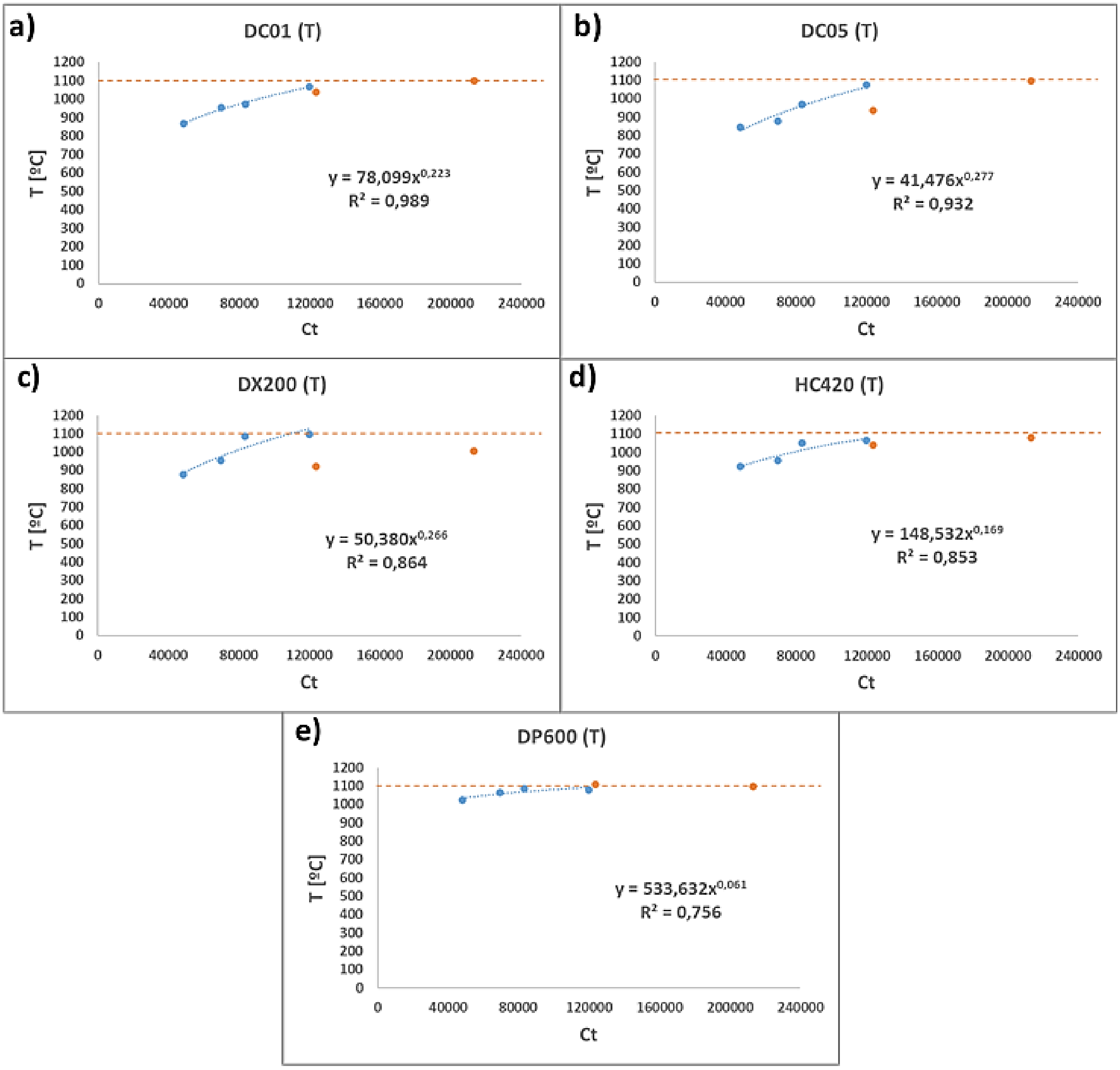

Figure 4.12 - Fitting graphs for the temperature

4.3. Sensitivity analysis

In order to better understand the evolution of the torque and of the temperature with the process parameters, a series of 3D graphs were plotted, based on the analytical results from equations (4.5) and (4.6), against the rotational speed and the tool diameter. In each 3D graph, the torque and temperature evolutions were represented by a surface, determined using the equations in the graphs of Figure 4.9, Figure 4.10 and Figure 4.12. Since mathematical modelling was used to plot the surfaces, the range of process parameters considered in this analysis was extended beyond the process parameter window considered in the experimental work (see Table 4.1). In each graph were also plotted, the experimental results, represented by dots, for comparison. In the next, those results are analysed, and based on it, the most influencing parameter on the thermomechanical conditions developed during welding is determined.

Table 4.1 - Process parameters for tri-dimensional graphs

Rotational Speed [rpm]	Tool Diameter [mm]
870	10 / 12 / 14 / 16 / 18
1150	10 / 12 / 14 / 16 / 18
1500	10 / 12 / 14 / 16 / 18

4.3.1. Torque versus process parameters

In Figure 4.13 are represented the maximum and stabilized torque percentual differences, for each base material, when the tool rotational speed and the tool diameter were increased by a factor of 75%. The values of torque were calculated using the model equations obtained previously (Figure 4.9 and Figure 4.10). The grey bar represents the direct difference between the values achieved. Due to a linear approach on maximum/stabilized torque, the evolution is equal, for both process output variables, regardless of the base material. From the figure it is possible to conclude that the tool diameter has a greater influence on the torque, than the rotational speed, since increasing its value in 75% induces a change in torque of 206.3%. On the other hand, by increasing the rotational speed in 75%, promoted a decrease in torque of only 42.9%. These results were also reported, for all materials, when analysing the maximum and stabilized torque evolution with process parameters in Figures Figure 4.4, Figure 4.5 and Figure 4.6.

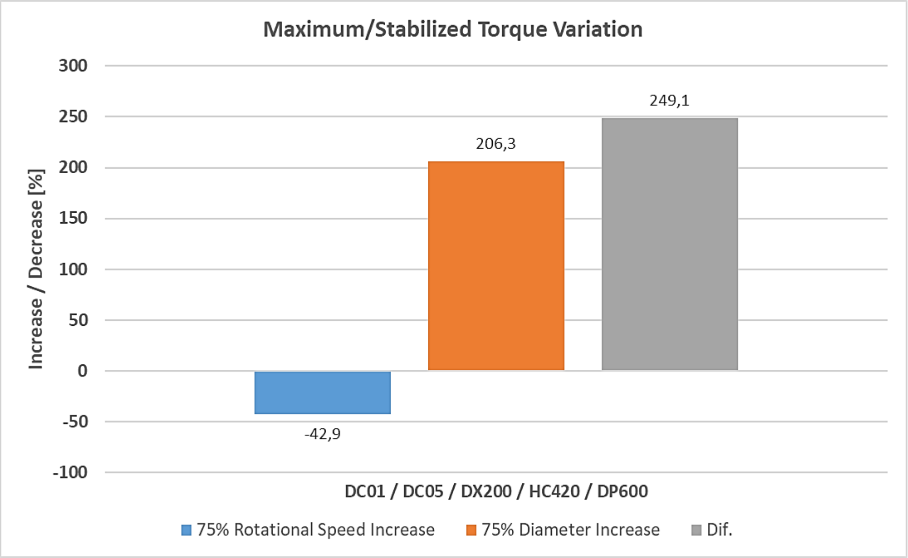

Figure 4.13 - Individual influence of process parameters in maximum/stabilized torque

The results obtained, relative to the evolution of the maximum and stabilized torque with process parameters, are shown in Figures Figure 4.14 and Figure 4.15, respectively. For comparison, the same colour map scale was used for all the surfaces in the graphs.

In Figure 4.14, where are displayed the results relative to the maximum torque, it is possible to observe that the maximum torque evolution with process parameters follows the same trend, for all the base materials, including the DX200 steel. More precisely, irrespective of the base material, the lowest M_{max} value was always registered for the lowest tool diameter and the highest rotational speed. A decrease of the maximum torque values when increasing the rotational speed and/or decreasing the tool diameter may be also noticed for all the base materials. However, it is also noticeable, that the impact of the tool diameter on the torque evolution is stronger than that of the tool rotational speed.

In Figure 4.15 are represented the surfaces relative to the stabilized torque evolution. Analysing the results it is possible depict the same trends as in the maximum torque. Also, between the materials, a similar evolution and values are achieved. This similarity was previewed when analysing Figure 4.2 for the evolution of the experimental values from stabilized torque and in Figure 4.11, where the K_M values obtained for the stabilized torque are compared for the base materials, highlighting its similarity.

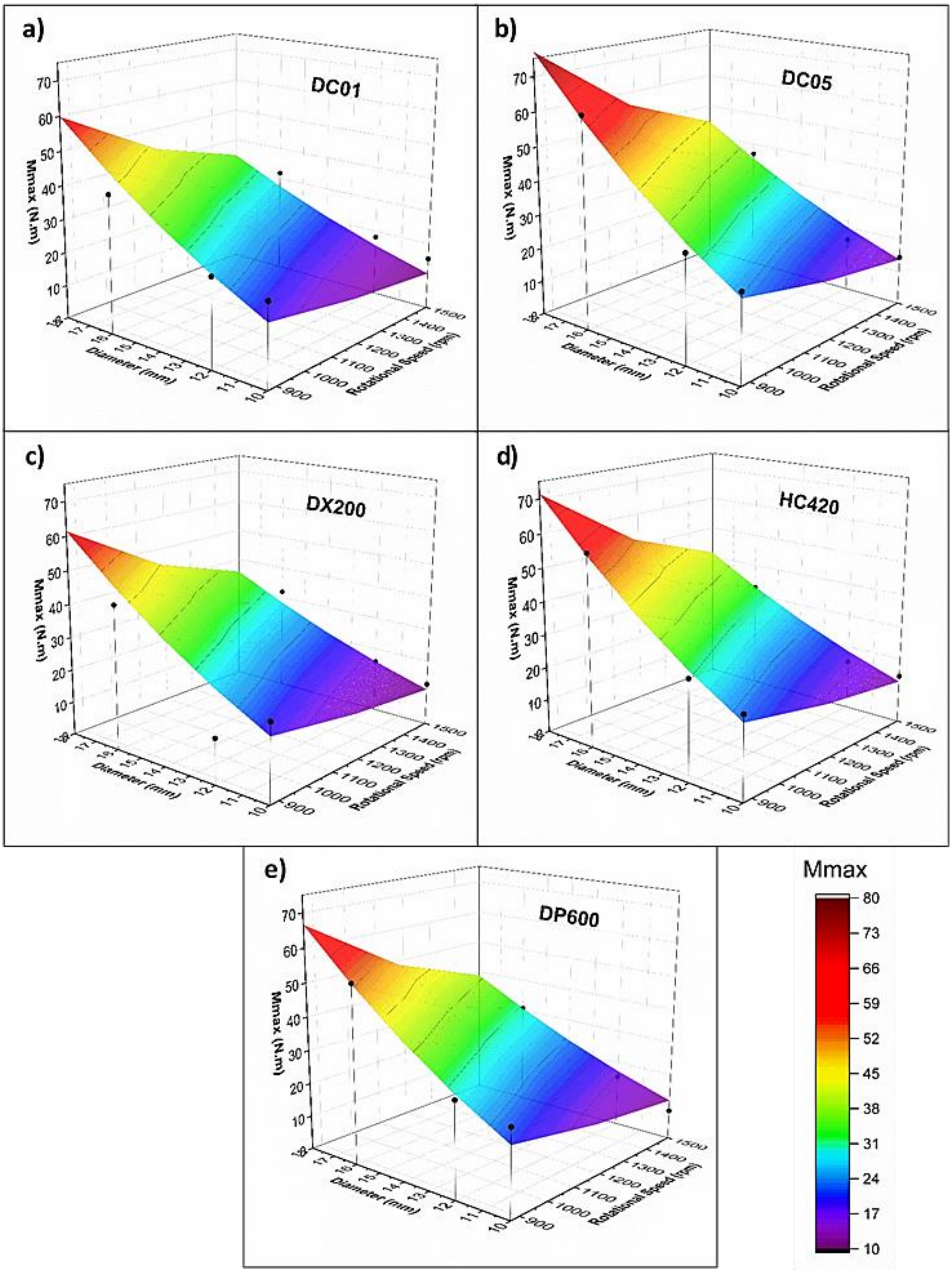

Figure 4.14 – Tri-dimensional graphs for maximum torque

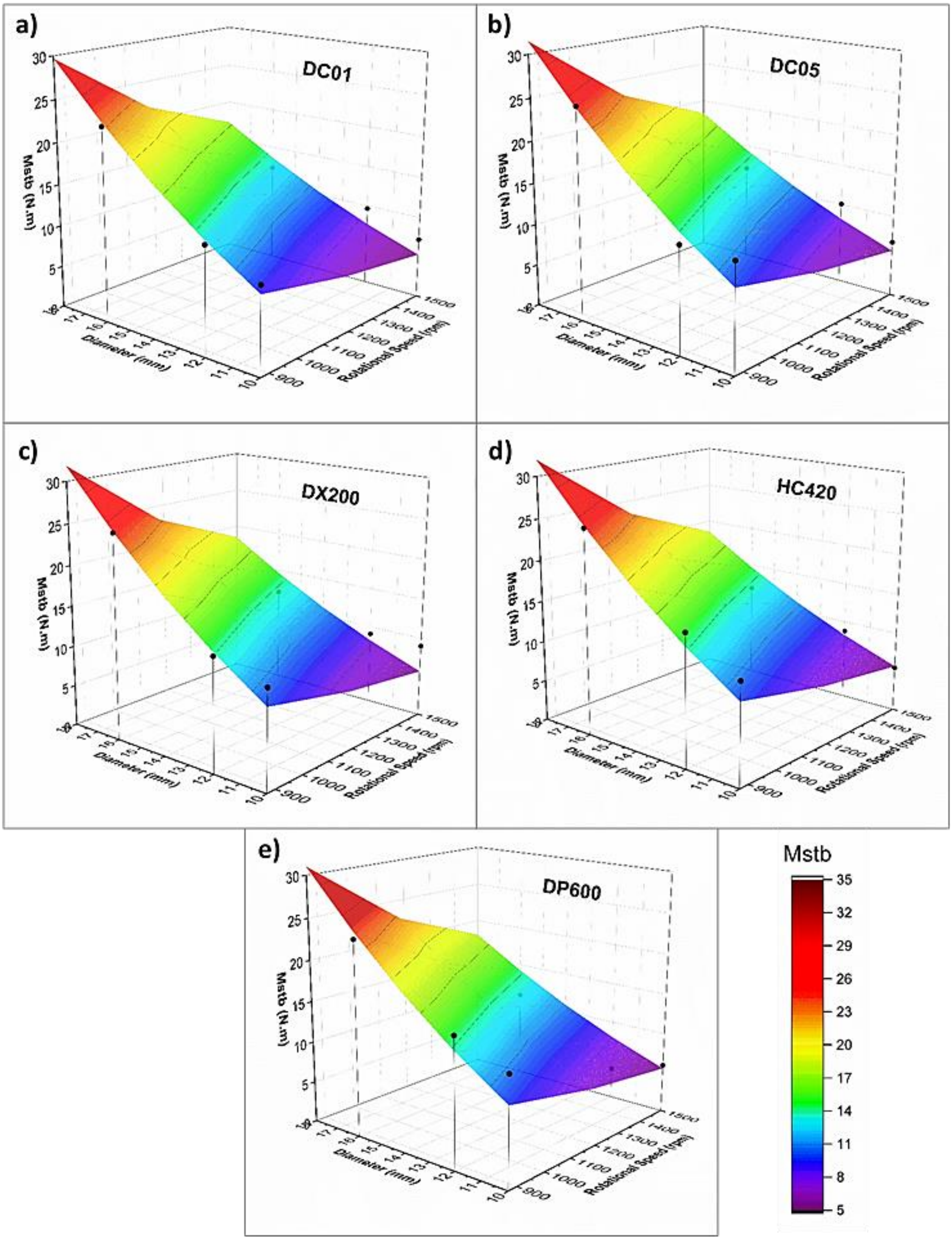

Figure 4.15 – Tri-dimensional graphs for stabilized torque

4.3.2. Temperature versus process parameters

The model surfaces for the temperature evolution with process parameters are represented in Figure 4.16. These graphs show important dissimilarities in temperature evolution with process parameters, for the different base materials. Actually, the figure shows that the temperature sensitivity to the process parameters diminishes as the strength of the alloy being welded increases, i.e., meanwhile for the DC01 and DC05 steels (Figure 4.16 a) and b)), the temperature deeply varies when varying the process parameters, for the DP600 (Figure 4.16 e)), the maximum temperature attained was always the same, independent of the process parameters. More precisely, for this steel, which was the highest strength material tested, maximum temperatures values varying between 1030 and 1100 ºC (threshold) were achieved. This corresponds, as shown, to an almost flat surface within a high temperature region.

In the figure are also represented, for each base material, the threshold temperature, corresponding to a flat surface at 1100 ºC. When comparing the experimental results with the model surfaces, it is noticeable a larger gap in the DC05 steel for the PL16 at 870 rpm, as analysed in Figure 4.12, of which may be associated with a temperature acquisition error.

It is also important to notice that, for the steels with process parameters dependent heat generation (DC01 and DC05), the maximum temperatures were attained when large diameter tools were combined with high rotational speeds. The figure also shows that the tool diameter had stronger influence on the temperature evolution than the rotational speed. In order to better illustrate this conclusion, in Figure 4.17 is shown the temperature increase calculated, for each base material, when the tool rotational speed and the tool diameter were increased by a factor of 75%, similarly to Figure 4.13, for maximum/stabilized torque. The immediate conclusion withdrawn from Figure 4.17 is that the diameter has a greater influence in the temperature increase when compared with the rotational speed. The grey bars represent the direct difference between the percentage values achieved for each case. The 75% diameter increase promotes an as high as a 33,7% temperature raise, for the DC05 steel, while the rotational speed increase promotes a maximum 16,8% temperature raise, for the same material, which represents a 16,9% difference. In the same graph, it is also noticeable a lower increase in temperature values for the higher strength materials, according to the true stress-strain curves showed in Figure 3.1.

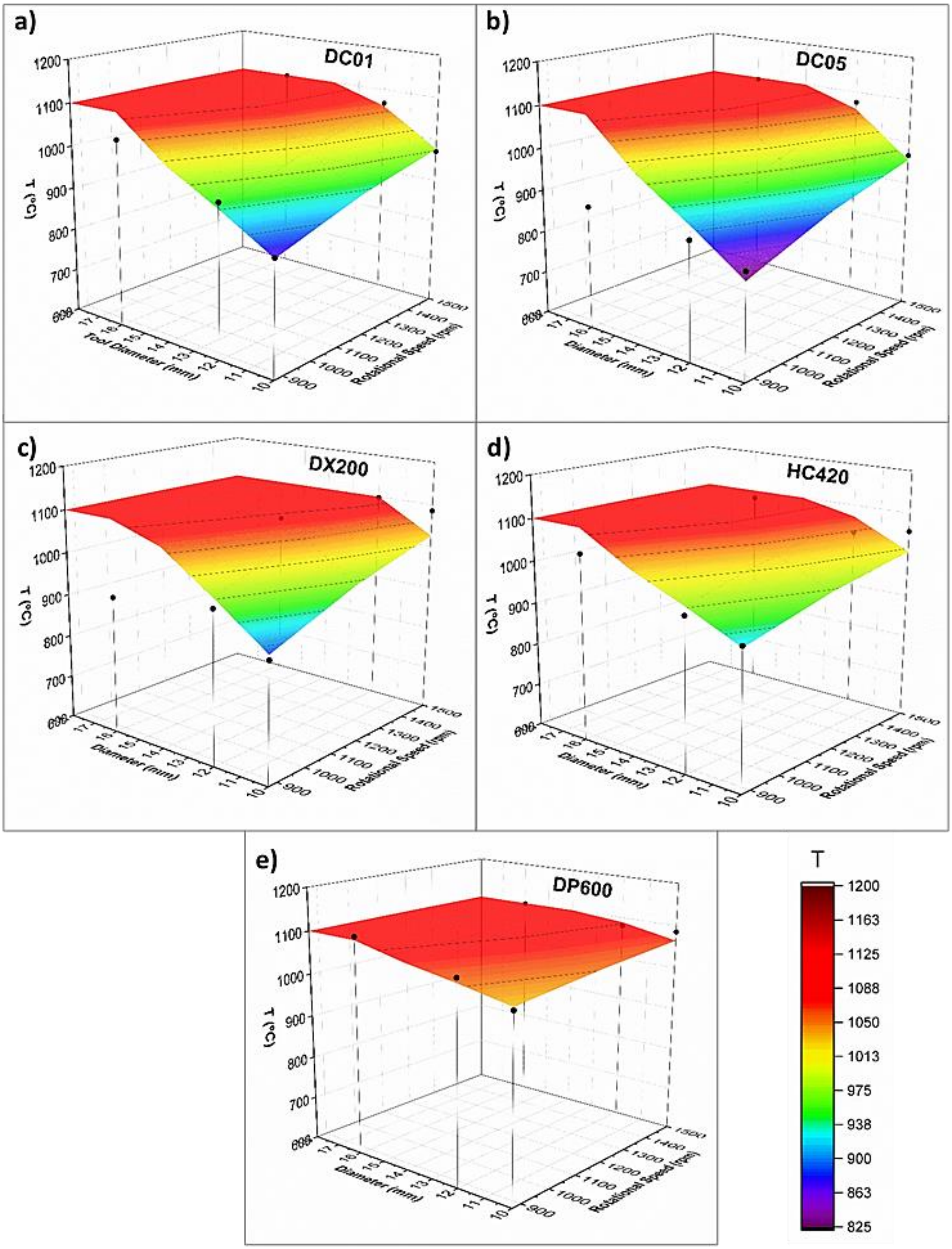

Figure 4.16 – Tri-dimensional graphs for temperature

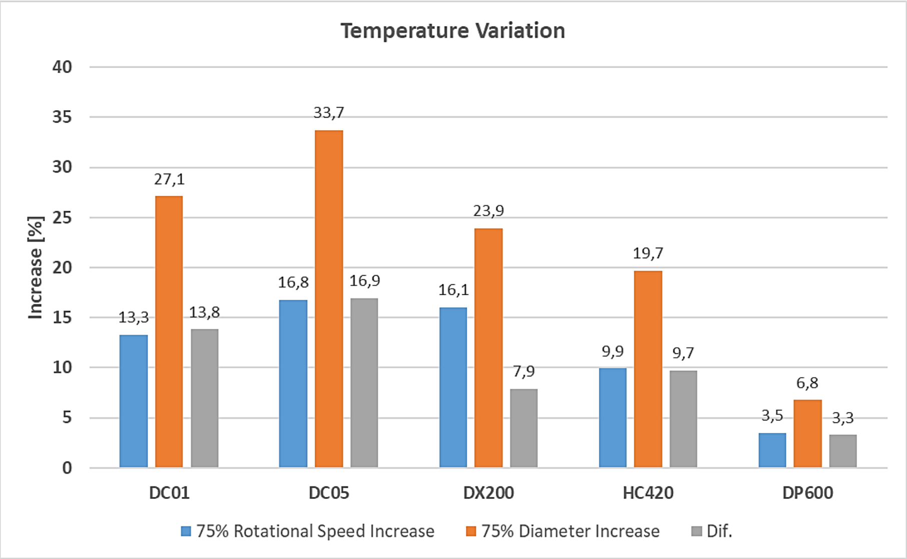

Figure 4.17 - Individual influence of process parameters in temperature

5. CONCLUSIONS

The main objective of this work was to analyse the torque and temperature evolutions in several steels when welded with a pinless tool for different rotational speeds and tool diameters. Later, the feasibility of a model capable of predicting torque and temperature values was tested. From this work, the following conclusions can be withdrawn:

- The tool diameter has a strong influence on both the maximum and stabilized torques, irrespective of the rotational speed and base material welded. When increasing the tool diameter, the torque values increase.
- The rotational speed increase leads to a decrease of both the maximum and stabilized torques, irrespective of the tool diameter and base material;
- For lower rotational speed (870 rpm) the temperature increases with the tool diameter, showing differences in values for the different materials. For the highest rotational speed (1500 rpm), the temperature is less sensitive to the tool diameter, presenting similar values for all the base materials. The temperatures are generally higher for the higher rotational speed, except for the DP600 steel, where the temperature evolutions at 870 and 1500 rpm are very similar. It is also concluded that a threshold in temperature 1100 ºC is reached;
- When correlating the temperature with the maximum/stabilized torque it is possible to conclude that an increase in rotational speed promoted a simultaneous increase in temperature and a decrease in torque, while an increase in tool diameter promoted an increase in both temperature and torque;
- The model chosen demonstrated a very good accuracy in predicting both maximum and stabilized torque, achieving high values of Pearson correlation coefficient;
- For the temperature, the model approach was not as efficient has for the torque, achieving slightly lower fitting values. Some errors in temperature acquisition may also be affecting the correlation between the model and the experimental results;

- Further analysis showed that the tool diameter has higher influence on the temperature increase than the rotational speed. For both the maximum and the stabilized torques it was shown that the rotational speed increase promotes a decrease in torque.

5.1. Future works

Further analysis can be done based on the results obtained in current work. A few suggestions of future works may include:

- To perform a metallographic analysis of the welds, aiming to corroborate the results obtained and also to find possible justification for some unexpected results;
- To develop a more accurate technique for temperature acquisition;
- To execute test with a wider/different range of process parameters.

BIBLIOGRAPHY

Andrade, D. G., Leitão, C., Dialami, N., Chiumenti, M., & Rodrigues, D. M. (2020a). Analysis of contact conditions and its influence on strain rate and temperature in Friction Stir Welding. *International Journal of Mechanical Sciences*, 106095. https://doi.org/10.1016/j.ijmecsci.2020.106095

Andrade, D. G., Leitão, C., Dialami, N., Chiumenti, M., & Rodrigues, D. M. (2020b). Modelling torque and temperature in friction stir welding of aluminium alloys. *International Journal of Mechanical Sciences*, *182*, 105725. https://doi.org/10.1016/j.ijmecsci.2020.105725

Andrade, D. G., Leitão, C., & Rodrigues, D. M. (2018). Properties of lap welds in low carbon galvanized steel produced by tool assisted friction welding. *Journal of Materials Processing Technology*, *260*, 77–86. https://doi.org/10.1016/j.jmatprotec.2018.05.018

Andrade, D. G., Leitão, C., & Rodrigues, D. M. (2019). Influence of base material characteristics and process parameters on frictional heat generation during Friction Stir Spot Welding of steels. *Journal of Manufacturing Processes*, *43*, 98–104. https://doi.org/10.1016/j.jmapro.2019.05.015

Arora, A., Nandan, R., Reynolds, A. P., & DebRoy, T. (2009). Torque, power requirement and stir zone geometry in friction stir welding through modeling and experiments. *Scripta Materialia*, *60*(1), 13–16. https://doi.org/10.1016/j.scriptamat.2008.08.015

Awang, M., & Mucino, V. H. (2010). Energy generation during friction stir spot welding (FSSW) of Al 6061-T6 plates. *Materials and Manufacturing Processes*, *25*(1–3), 167–174. https://doi.org/10.1080/10426910903206758

Baek, S. W., Choi, D. H., Lee, C. Y., Ahn, B. W., Yeon, Y. M., Song, K., & Jung, S. B. (2010). Microstructure and mechanical properties of friction stir spot welded galvanized steel. *Materials Transactions*, *51*(5), 1044–1050. https://doi.org/10.2320/matertrans.M2009337

Bakavos, D., Chen, Y., Babout, L., & Prangnell, P. (2011). Material interactions in a novel pinless tool approach to friction stir spot welding thin aluminum sheet. *Metallurgical and Materials Transactions A: Physical Metallurgy and Materials Science*, *42*(5), 1266–1282. https://doi.org/10.1007/s11661-010-0514-x

Colligan, K. J., & Mishra, R. S. (2008). A conceptual model for the process variables related to heat generation in friction stir welding of aluminum. *Scripta Materialia*, *58*(5), 327–331. https://doi.org/10.1016/j.scriptamat.2007.10.015

Cox, C. D., Aguilar, J. R., Ballun, M. C., Strauss, A. M., & Cook, G. E. (2014). The application of a pinless tool in friction stir spot welding: An experimental and numerical study. *Proceedings of the Institution of Mechanical Engineers, Part D: Journal of Automobile Engineering*, *228*(11), 1359–1370. https://doi.org/10.1177/0954407013517374

Cox, C. D., Gibson, B. T., Strauss, A. M., & Cook, G. E. (2012). Effect of pin length and rotation rate on the tensile strength of a friction stir spot-welded al alloy: A contribution to automated production. *Materials and Manufacturing Processes*, *27*(4), 472–478. https://doi.org/10.1080/10426914.2011.585503

De Leon, M., & Shin, H. S. (2016). Material flow behaviours during friction stir spot welding of lightweight alloys using pin and pinless tools. *Science and Technology of Welding and Joining*, *21*(2), 140–146. https://doi.org/10.1179/1362171815Y.0000000075

Freeney, T. A., Sharma, S. R., & Mishra, R. S. (2006, April 3). Effect of welding parameters on properties of 5052 Al friction stir spot welds. *SAE Technical Papers*. https://doi.org/10.4271/2006-01-0969

Jedrasiak, P., & Shercliff, H. R. (2019). Small strain finite element modelling of friction stir spot welding of Al and Mg alloys. *Journal of Materials Processing Technology*, *263*, 207–222. https://doi.org/10.1016/j.jmatprotec.2018.07.031

Khosa, S. U., Weinberger, T., & Enzinger, N. (2010). Thermo-mechanical investigations during Friction Stir Spot Welding (FSSW) of AA6082-T6. In *Welding in the World* (Vol. 54, Issues 5–6, pp. R134–R146). Springer Verlag. https://doi.org/10.1007/BF03263499

Lakshminarayanan, A. K., Annamalai, V. E., & Elangovan, K. (2015). Identification of optimum friction stir spot welding process parameters controlling the properties of low carbon automotive steel joints. *Journal of Materials Research and Technology*, *4*(3), 262–272. https://doi.org/10.1016/j.jmrt.2015.01.001

Leitão, C., Louro, R., & Rodrigues, D. M. (2012a). Analysis of high temperature plastic behaviour and its relation with weldability in friction stir welding for aluminium alloys AA5083-H111 and AA6082-T6. *Materials and Design*, *37*, 402–409. https://doi.org/10.1016/j.matdes.2012.01.031

Leitão, C., Louro, R., & Rodrigues, D. M. (2012b). Using torque sensitivity analysis in accessing Friction Stir Welding/Processing conditions. *Journal of Materials Processing Technology*, *212*(10), 2051–2057. https://doi.org/10.1016/j.jmatprotec.2012.05.009

Longhurst, W. R., Strauss, A. M., Cook, G. E., & Fleming, P. A. (2010). Torque control of friction stir welding for manufacturing and automation. *International Journal of Advanced Manufacturing Technology*, *51*(9–12), 905–913. https://doi.org/10.1007/s00170-010-2678-3

Mazzaferro, C. C. P., Rosendo, T. S., Tier, M. A. D., Mazzaferro, J. A. E., Dos Santos, J. F., & Strohaecker, T. R. (2015). Microstructural and mechanical observations of galvanized TRIP steel after friction stir spot welding. *Materials and Manufacturing Processes*, *30*(9), 1090–1103. https://doi.org/10.1080/10426914.2015.1004699

Mira-Aguiar, T., Verdera, D., Leitão, C., & Rodrigues, D. M. (2016). Tool assisted friction welding: A FSW related technique for the linear lap welding of very thin steel plates. *Journal of Materials Processing Technology*, *238*, 73–80. https://doi.org/10.1016/j.jmatprotec.2016.07.006

Mousavizade, S. M., & Pouranvari, M. (2019). Projection friction stir spot welding: a pathway to produce strong keyhole-free welds. *Science and Technology of Welding and Joining*, *24*(3), 256–262. https://doi.org/10.1080/13621718.2018.1521068

Rai, R., De, A., Bhadeshia, H. K. D. H., & DebRoy, T. (2011). Review: Friction stir welding tools. *Science and Technology of Welding and Joining*, *16*(4), 325–342. https://doi.org/10.1179/1362171811Y.0000000023

Rodrigues, A., Rodrigues, D., & Leitão, C. (2017). *Análise das Condições Termomecânicas em Tool Assisted Friction Welding*. Universidade de Coimbra.

Sakano, R., Murakami, K., Yamashita, K., Hyde, T., & Fujimoto, M. (2001). *Development of spot FSW robot system for automobile body members. In Third International*

Symposium on Friction Stir Welding (2001).

Santella, M., Brown, E., Pozuelo, M., Pan, T. Y., & Yang, J. M. (2012). Details of Mg-Zn reactions in AZ31 to galvanised mild steel ultrasonic spot welds. *Science and Technology of Welding and Joining*, *17*(3), 219–224. https://doi.org/10.1179/1362171811Y.0000000098

Schmidt, H., Hattel, J., & Wert, J. (2004). An analytical model for the heat generation in friction stir welding. *Modelling and Simulation in Materials Science and Engineering*, *12*(1), 143–157. https://doi.org/10.1088/0965-0393/12/1/013

Shen, Z., Ding, Y., & Gerlich, A. P. (2019). Advances in friction stir spot welding. In *Critical Reviews in Solid State and Materials Sciences* (pp. 1–78). Taylor and Francis Inc. https://doi.org/10.1080/10408436.2019.1671799

Tozaki, Y., Uematsu, Y., & Tokaji, K. (2010). A newly developed tool without probe for friction stir spot welding and its performance. *Journal of Materials Processing Technology*, *210*(6–7), 844–851. https://doi.org/10.1016/j.jmatprotec.2010.01.015

Yazdi, S. R., Beidokhti, B., & Haddad-Sabzevar, M. (2019). Pinless tool for FSSW of AA 6061-T6 aluminum alloy. *Journal of Materials Processing Technology*, *267*, 44–51. https://doi.org/10.1016/j.jmatprotec.2018.12.005

Zuzarte, M., Rodrigues, D., & Leitão, C. (2018). *Ligação de aços com baixo teor em carbono pelo processo Tool Assisted Friction Welding*.

APPENDIX A

Table A.1 - Maximum temperature, maximum torque and stabilized torque values obtained from experimental tests

Materials	Rotational Speed [rpm]	Diameter [mm]	T_{max} [ºC]	M_{max} [N.m]	M_{stb} [N.m]
DC01	870	10	867,15	24,21	10,19
		12	953,24	26,16	12,74
		16	1037,80	40,91	23,03
	1500	10	971,28	15,35	7,23
		12	1067,02	18,10	9,62
		16	1098,75	31,84	12,26
DC05	870	10	843,99	25,56	12,63
		12	876,82	31,37	12,60
		16	937,05	61,80	25,13
	1500	10	969,94	14,50	6,71
		12	1075,24	15,95	10,04
		16	1095,74	36,78	11,95
DX200	870	10	876,30	23,02	11,95
		12	954,12	29,65	13,67
		16	921,34	43,24	24,98
	1500	10	1085,43	12,69	9,03
		12	1098,10	15,84	9,24
		16	1004,09	31,96	11,94
HC420	870	10	923,47	24,35	12,13
		12	956,79	29,51	15,81
		16	1040,82	57,33	24,97
	1500	10	1049,73	15,66	5,51

		12	1064,05	15,06	8,75
		16	1080,96	32,74	11,79
DP600	870	10	1023,62	25,43	13,00
		12	1064,75	28,10	15,52
		16	1107,96	52,93	23,61
	1500	10	1085,59	8,64	5,95
		12	1080,55	15,35	9,37
		16	1098,55	30,63	10,83